A dual function of the IDA peptide in regulating cell separation and modulating plant immunity at the molecular level

Vilde Olsson Lalun[1], Maike Breiden[§2], Sergio Galindo-Trigo[1§], Elwira Smakowska-Luzan[3], Rüdiger Simon[3] and Melinka A. Butenko[1*]

[1]Section for Genetics and Evolutionary Biology, Department of Biosciences, University of Oslo, 0316 Oslo, Norway

[2]Institute for Developmental Genetics and Cluster of Excellence on Plant Sciences, Heinrich Heine University, Universitätsstraße 1, 40225 Düsseldorf, Germany

[3]Gregor Mendel Institute (GMI), Austrian Academy of Sciences, Vienna Biocenter (VBC), Dr Bohr-Gasse 3, 1030 Vienna, Austria

[§]Equal contribution

*Corresponding author; email: m.a.butenko@ibv.uio.no

Abstract:

The abscission of floral organs and emergence of lateral roots in Arabidopsis is regulated by the peptide ligand INFLORESCENCE DEFICIENT IN ABSCISSION (IDA) and the receptor protein kinases HAESA (HAE) and HAESA-LIKE 2 (HSL2). During these cell separation processes, the plant induces defense-associated genes to protect against pathogen invasion. However, the molecular coordination between abscission and immunity has not been thoroughly explored. Here we show that IDA induces a receptor-dependent release of cytosolic calcium ions (Ca^{2+}) and apoplastic production of reactive oxygen species, which are signatures of early defense responses. In addition, we find that IDA promotes late defense responses by the transcriptional upregulation of genes known to be involved in immunity. When comparing the IDA induced early immune responses to known immune responses, such as those elicited by flagellin22 treatment, we observe both similarities and differences. We propose a molecular mechanism by which IDA promotes signatures of an immune response in cells destined for separation to guard them from pathogen attack.

31

32

33

34 ## Introduction

35 All multicellular organisms require tightly regulated cell-to-cell communication during development and
36 adaptive responses. In addition to hormones, plants use small-secreted peptide ligands to regulate
37 these highly coordinated events of growth, development and responses to abiotic and biotic stress
38 (Matsubayashi, 2011; Olsson et al., 2018). In plants, organ separation or abscission, involves cell
39 separation between specialized abscission zone (AZ) cells and enables the removal of unwanted or
40 diseased organs in response to endogenous developmental signals or environmental stimuli.
41 *Arabidopsis thaliana* (Arabidopsis) abscise floral organs (stamen, petals and sepals) after pollination, and
42 this system has been used as a model to study the regulation of cell separation and abscission (Bleecker
43 & Patterson, 1997). Precise cell separation also occurs during the emergence of new lateral root (LR)
44 primordia, root cap sloughing, formation of stomata and radicle emergence during germination
45 (Roberts et al., 2000). In Arabidopsis, the INFLORESCENCE DEFICIENT IN ABSCISSION (IDA) peptide
46 mediated signaling system ensures the correct spatial and temporal abscission of sepals, petals, and
47 stamens. The IDA protein shares a conserved C-terminal domain with the other 7 IDA-LIKE (IDL)
48 members (Butenko et al., 2003, Vie et al., 2015) which is processed to a functional 12 amino acid
49 hydroxylated peptide (Butenko et al., 2014). The abscission process is regulated by the production and
50 release of IDA, which binds the genetically redundant plasma membrane (PM) localized receptor kinases
51 (RKs), HAESA (HAE) and HAESA-LIKE 2 (HSL2). IDA binding to HAE and HSL2 promotes receptor
52 association with members of the co-receptor SOMATIC EMBRYOGENESIS RECEPTOR KINASE (SERK)
53 family and further downstream signaling leading to cell separation events. (Cho et al., 2008; Meng et
54 al., 2016; Santiago et al., 2016; Stenvik et al., 2008). A deficiency in the IDA signaling pathway prevents
55 the expression of genes encoding secreted cell wall remodeling and hydrolase enzymes thus hindering
56 floral organs to abscise (Butenko et al., 2003; Cho et al., 2008; Kumpf et al., 2013; Xiangzong Meng et
57 al., 2016; Niederhuth et al., 2013; Stenvik et al., 2008; Isaiah Taylor & John C. Walker, 2018).
58 Interestingly, components of the IDA signaling pathway control different cell separation events during
59 Arabidopsis development. IDA signaling through HAE and HSL2 regulates cell wall remodeling genes in
60 the endodermal, cortical, and epidermal tissues overlaying the LR primordia during LR emergence
61 (Kumpf et al., 2013). In addition, IDL1 signals through HSL2 to regulate cell separation during root cap
62 sloughing (Shi et al., 2018).

63 Plant cell walls act as physical barriers against pathogenic invaders. The cell-wall processing and
64 remodeling that occurs during abscission leads to exposure of previously protected tissue. This provides

65 an entry point for phytopathogens thereby increasing the need for an effective defense system in these
66 cells (Agustí et al., 2009). Indeed, it has been shown that AZ cells undergoing cell separation express
67 defense genes and it has been proposed that they function in protecting the AZ from infection after
68 abscission has occurred (Cai & Lashbrook, 2008; Niederhuth et al., 2013). *mIDA* elicits the production of
69 Reactive Oxygen Species (ROS) in *Nicotiana benthamiana* (*N.benthamiana*) leaves transiently expressing
70 the HAE or HSL2 receptor (Butenko et al., 2014). As a consequence of defense responses, ROS occurs in
71 the apoplast and is involved in regulating the cell wall structure by producing cross-linking of cell wall
72 components in the form of hydrogen peroxide (H_2O_2) or act as cell wall loosening agents in the form of
73 hydroxyl radical ($^{\cdot}OH$)radicals (Kärkönen & Kuchitsu, 2015). ROS may also serve as a direct defense
74 response by their highly reactive and toxic properties (Kärkönen & Kuchitsu, 2015). In addition, ROS may
75 act as a secondary signaling molecule enhancing intracellular defense responses as well as contributing
76 to the induction of defense related genes (Reviewed in (Castro et al., 2021)). In Arabidopsis, apoplastic
77 ROS is mainly produced by a family of NADPH oxidases located in the plasma membrane known as
78 RESPIRATORY BURST OXIDASE PROTEINs (RBOHs) (Torres & Dangl, 2005). The production of ROS is often
79 found closely linked to an increase in the concentration of cytosolic Ca^{2+} ($[Ca^{2+}]_{cyt}$), where the interplay
80 between these signaling molecules is observed in immunity across kingdoms (Kadota et al., 2015;
81 Steinhorst & Kudla, 2013). Interestingly, ROS and $[Ca^{2+}]_{cyt}$ are known signaling molecules acting
82 downstream of several peptide ligand-receptor pairs. This includes the endogenous PAMPs ELICITOR
83 PEPTIDE(PEP)1, PEP2 and PEP3 which function as elicitors of systemic responses against pathogen attack
84 and herbivory (Huffaker et al., 2006; Ma et al., 2012; Qi et al., 2010), as well as the pathogen derived
85 peptide ligands flagellin22 (flg22) and Ef-Tu which bind and activate defense related RKs in the PM of
86 the plant cell (Felix et al., 1999; Gómez-Gómez et al., 1999; Ranf et al., 2011).

87 The interplay between ROS and $[Ca^{2+}]_{cyt}$ has been well studied in the flg22 induced signaling system. The
88 flg22 peptide interacts with the extracellular domain of the FLAGELLIN SENSING2 (FLS2) receptor kinase,
89 which rapidly leads to an increase in $[Ca^{2+}]_{cyt}$ (Ranf et al., 2011). In a resting state, the co-receptor
90 BRASSINOSTEROID INSENSITIVE1-ASSOCIATED RECEPTOR KINASE1/SERK3) (BAK1) and the cytoplasmic
91 kinase BOTRYTIS-INDUCED KINASE1 (BIK1) form a complex with FLS2. Upon binding of flg22 to the FLS2
92 receptor, BIK1 is released from the receptor complex and activates intracellular signaling molecules
93 through phosphorylation, among other, the PM localized RBOHD (Kadota et al., 2014; Li et al., 2014).
94 flg22 induced apoplastic ROS production binds to PM localized Ca^{2+} channels on neighboring cells,
95 activating Ca^{2+} influx into the cytosol. The cytosolic Ca^{2+} may bind to CALCIUM DEPENDENT PROTEIN
96 KINASE5 (CDPKs) regulating RBOHD activity through phosphorylation. The Ca^{2+} dependent
97 phosphorylation of RBOH enhances ROS production, which in turn leads to a propagation of the
98 ROS/Ca^{2+} signal through the plant tissue (Dubiella et al., 2013)

99 A rapid increase in $[Ca^{2+}]_{cyt}$ is not only observed in peptide-ligand induced signaling. Similar $[Ca^{2+}]_{cyt}$
100 changes are observed as responses to developmental signals, such as extracellular auxin and
101 environmental signals such as high salt conditions and drought(reviewed in (Kudla et al., 2018)). Also,
102 $[Ca^{2+}]_{cyt}$ signals are observed in single cells during pollen tube and root hair growth (Monshausen et al.,
103 2008; Sanders et al., 1999). How cells decipher the $[Ca^{2+}]_{cyt}$ changes into a specific cellular response is
104 still largely unknown, however the cell contains a large toolkit of Ca^{2+} sensor proteins that may affect
105 cellular function through changes in protein phosphorylation and gene expression. Each Ca^{2+} binding
106 protein has specific affinities for Ca^{2+} allowing them to respond to different Ca^{2+} concentrations
107 providing a specific cellular response (Geiger et al., 2010; Scherzer et al., 2012).
108
109 Due to our previous studies showing IDA induced apoplastic ROS production (Butenko et al., 2014), and
110 the known link between ROS and $[Ca^{2+}]_{cyt}$ response observed for other ligands such as flg22 (Dubiella et
111 al., 2013), we sought to investigate if IDA induces a release of $[Ca^{2+}]_{cyt}$. Here we report that IDA is able
112 to induce an intracellular release of Ca^{2+} in Arabidopsis root tips as well as in the AZ. Therefore, we
113 aimed to understand how the observed production of ROS and Ca^{2+} is involved in the IDA-HAE/HSL2
114 signaling pathway, either by being a part of the developmental process of abscission or as a part of a
115 suggested involvement of IDA in regulating plant defense (Patharkar et al., 2017). We show that a range
116 of biotic and abiotic signals can induce *IDA* expression and we demonstrate that the IDA signal
117 modulates responses of plant immune signaling. We propose that, in addition to regulating cell
118 separation, IDA plays a role in enhancing a defense response in tissues undergoing cell separation thus
119 providing the essential need for enhanced defense responses in tissue during the cell separation event.
120
121

122 ## Results:

123 ### IDA induces apoplastic production of ROS and elevation in cytosolic calcium-ion concentration

124 We have previously shown that a 12 amino acids functional IDA peptide, hereby referred to as mIDA
125 (Sup Table 1), elicits the production of a ROS burst in *N.benthamiana* leaves transiently expressing *HAE*
126 or *HSL2* (Butenko et al., 2014). To investigate whether mIDA could elicit a ROS burst in Arabidopsis, a
127 luminol-dependent ROS assay on *hae hsl2* mutant rosette leaves expressing the full length HAE receptor
128 under a constitutive promoter (*35S:HAE-YFP*) was performed. *hae hsl2 35S:HAE-YFP* leaf discs treated
129 with mIDA emitted extracellular ROS, whereas no response was observed in wild-type (WT) leaves most
130 likely due to the absence of *HAE* expression (Sup Fig. 1). Since rapid production of ROS is often linked to
131 an elevation in $[Ca^{2+}]_{cyt}$ (Steinhorst & Kudla, 2013), we aimed to investigate if mIDA could induce a

132 $[Ca^{2+}]_{cyt}$ response. We imaged Ca^{2+} in 10 days-old roots expressing the cytosolic localized fluorescent
133 Ca^{2+} sensor R-GECO1 (Keinath et al., 2015). As a positive control for $[Ca^{2+}]_{cyt}$ release we added 1mM
134 extracellular ATP (eATP), which leads to a $[Ca^{2+}]_{cyt}$ elevation in the root tip within a minute after
135 application (Fig. 1a) (Breiden et al., 2021). After application of 1µM mIDA, we detected an increase in
136 $[Ca^{2+}]_{cyt}$ (Fig. 1a and Movie 1). R-GECO1 fluorescence intensities normalized to background intensities
137 (ΔF/F) were measured from a region of interest (ROI) covering the meristematic and elongation zone of
138 the root and revealed that the response starts 4-5 minutes after application of the mIDA peptide and
139 lasts for 7-8 minutes (Fig. 1a). The signal initiated in the root meristematic zone from where it spread
140 toward the elongation zone and root tip, a second wave was observed in the meristematic zone
141 continuing with Ca^{2+} spikes. The signal amplitude was at a maximum within the elongation zone and
142 decreased as the signal spread (Fig. 1a).

143 The $[Ca^{2+}]_{cyt}$ response in roots to the bacterial elicitor flg22 has previously been studied using the R-
144 GECO1 sensor (Keinath et al., 2015). To better understand the specificity of the mIDA induced Ca^{2+}
145 response, we aimed to compare the Ca^{2+} dynamics in mIDA treated roots to those treated with flg22.
146 We observed striking differences in the onset and distribution of the Ca^{2+} signals. Analysis of roots
147 treated with 1 µM flg22 showed that the Ca^{2+} signal initiated in the root elongation zone from where it
148 spread toward the meristematic zone as a single wave and that the signal amplitude was at a maximum
149 within the elongation zone and decreased as the signal spread (Fig. 1b, Movie 2). These observations
150 indicate differences in tissue specificity of Ca^{2+} responses between mIDA and flg22, which we
151 hypothesize depend on the cellular distribution of their cognate receptors. Indeed, when investigating
152 the promoter activity of the *HAE*, *HSL2* and *FLS2* receptors by cloning the promoters fused to the nuclear
153 localized YFP-derived fluorophore Venus protein (*pHAE:Venus-H2B*, *pHSL2:Venus-H2B* and
154 *pFLS2:Venus-H2B*) we observed a different pattern of fluorescent nuclei in the roots (Fig. 1c,d,e).
155 *pHAE:Venus-H2B* lines had fluorescent expression in the epidermis and stele of the elongation zone (Fig.
156 1c) and *pHSL2:Venus-H2B* lines in the lateral root cap, root tip and root meristem (Fig. 1d); while
157 fluorescent nuclei were observed in the stele of the elongation zone in *pFLS2:Venus-H2B lines* (Fig. 1e).
158 The different patterns of fluorescent nuclei observed for the three different receptor constructs could
159 indeed explain the differences in the Ca^{2+} signatures triggered by mIDA and flg22. However, the
160 receptors promoter activity show a broader expression pattern compared to the respective ligand
161 induced $[Ca^{2+}]_{cyt}$ responses, indicating additional regulating factors for the observed $[Ca^{2+}]_{cyt}$ response.

162 The flg22 induced $[Ca^{2+}]_{cyt}$ response is completely abolished in the *fls2* mutant (Ranf et al., 2011). To
163 investigate the dependency of the mIDA-induced response on HAE and HSL2, a cytosolic localized
164 Aequorin-based luminescence Ca^{2+} sensor (Aeq) was introduced into the *hae hsl2* mutant background
165 (Knight et al., 1991). The Aeq sensor was chosen due to the well-established use of this sensor in mutant

166 studies (Ranf et al., 2011) and due to problems with transgene silencing of the R-GECO1 reporter in *hae*
167 *hsl2* (not shown). The mIDA triggered increase in $[Ca^{2+}]_{cyt}$ was completely abolished in *hae hsl2 Aeq*
168 seedlings compared to WT *Aeq* expressing seedlings, indicating that the response observed is receptors
169 dependent (Sup Fig. 2a). Removing the last Asparagine of the mIDA peptide (IDAΔN69; Sup Table 1)
170 renders it inactive (Butenko et al., 2014). Seedlings treated with 1 µM IDAΔN69 did not show any
171 increase in $[Ca^{2+}]_{cyt}$ (Sup Fig. 2a). To investigate if the $[Ca^{2+}]_{cyt}$ increase triggered by mIDA was dependent
172 on extracellular Ca^{2+}, we pre-treated seedling with $LaCl_3$ and Ethylene glycol-bis (2-aminoethylether)- N,
173 N, N′,N′-tetraacetic acid (EGTA). $LaCl_3$ and EGTA are inhibitors that block plasma membrane localized
174 cation channels and chelate Ca^{2+} in the extracellular space, respectively (Knight et al., 1997). The mIDA
175 induced response was abolished in *Aeq*-seedlings pre-incubated in 2 mM EGTA or 1 mM $LaCL_3$ (Sup Fig.
176 2b), indicating that the mIDA dependent $[Ca^{2+}]_{cyt}$ response depends on Ca^{2+} from the extracellular space.

177 Next we set out to investigate whether mIDA would trigger an increase in $[Ca^{2+}]_{cyt}$ in floral AZ cells. We
178 utilized the Aeq expressing line and monitored $[Ca^{2+}]_{cyt}$ changes in flowers at different developmental
179 stages (see Sup Fig. 3a for developmental stages [floral positions]) to 1 µM mIDA. Interestingly, only
180 flowers at a the stage where there is an initial weakening of the AZ cell walls showed an increase in
181 $[Ca^{2+}]_{cyt}$ (Sup Fig. 3). Flowers treated with mIDA prior to cell wall loosening showed no increase in
182 luminescence (Sup Fig. 3), indicating that the mIDA triggered Ca^{2+} release in flowers correlates with the
183 onset of the abscission process and the increase in *HAE* and *HSL2* expression at the AZ (Cai & Lashbrook,
184 2008; Patharkar & Walker, 2015). Using plants expressing the R-GECO1 sensor we performed a detailed
185 investigation of the mIDA induced $[Ca^{2+}]_{cyt}$ response in flowers at position 6 which is the position where
186 initial cell wall loosening occurs. The AZ region was analyzed for signal intensity values and revealed that
187 the Ca^{2+} signal was composed of one wave (Fig. 2, Movie 3). The signal initiated close to the nectaries
188 and spread throughout the AZ and further into the floral receptacle. Flowers treated with 1 µM IDAΔN69
189 did not show any increase in $[Ca^{2+}]_{cyt}$ in the AZ or receptacle, while a clear Ca^{2+} wave could be detected
190 in the whole AZ, receptacle and proximal pedicel after treatment with eATP (Sup Fig.4, Sup Movie 2).
191 Detailed investigation of *HAE* and *HSL2* promoter activity in flowers at position 6 shows restricted
192 promoter activity to the AZ cells (Fig. 2b). The observed promoter activity correlates with the observed
193 mIDA induced $[Ca^{2+}]_{cyt}$ response.

194

195 **The ROS producing enzymes, RBOHD and RBOHF, are not involved in the developmental process of**
196 **abscission.**

197 ROS and Ca^{2+} are secondary messengers that can play a role in developmental processes involving cell
198 wall remodeling, but are also important players in plant immunity (Kärkönen & Kuchitsu, 2015). We

199 therefore set out to investigate if the IDA induced production of ROS and increase in $[Ca^{2+}]_{cyt}$ function in
200 the developmental process of abscission or if these signaling molecules form part of IDA modulated
201 plant immunity.

202 The IDA induced Ca^{2+} response depends on Ca^{2+} from extracellular space (Sup Fig. 2b). Ca^{2+} transport
203 over the plasma membrane is enabled by a variety of Ca^{2+} permeable channels, including the CYCLIC
204 NUCLEOTIDE GATED CHANNELs (CNGCs). Various CNGCs are known to be involved in peptide ligand
205 signaling in plants, including the involvement of CNGC6 and CNGC9 in CLAVATA3/EMBRYO
206 SURROUNDING REGION40 signaling in roots (Breiden et al., 2021), and CNGC17 In phytosulfokine
207 signaling (Ladwig et al., 2015). Using publicly available expression data we identified multiple CNGCs
208 expressed in the AZ of Arabidopsis (Cai & Lashbrook, 2008) (Sup Fig. 5a) and investigated if plants
209 carrying mutations in the *CNGSs* genes expressed in AZs showed a defect in floral organ abscission. We
210 observed no deficiency in floral abscission in the *cngc* mutants (Sup Fig. 5b), in contrast to what is
211 observed in the *hae hsl2* mutant where all floral organs are retained throughout the inflorescence. Ca^{2+}
212 partially activates members of the NOX family of NADPH oxidases (RBOHs), key producers of ROS
213 (Kadota et al., 2015). Two members of this family, *RBOHD* and *RBOHF* have high transcriptional levels in
214 the floral AZs (Cai & Lashbrook, 2008) and have been reported to be important in the cell separation
215 event during floral abscission in Arabidopsis (Lee et al., 2018). We therefore set out to investigate if ROS
216 production in AZ cells was dependent on RBOHD and RBOHF and to quantify to which degree these
217 NADPH oxidases were necessary for organ separation. We treated AZs with the ROS indicator, H2DCF-
218 DA, which upon contact with ROS has fluorescent properties, and observed ROS in both WT and to a
219 lower extent in *rbohd rbohdf* flowers. In addition, we observed normal floral abscission in the *rbohd*
220 *rbohf* double mutant flowers, indicated that neither ROS production in the AZ nor cell separation was
221 dependent on RBOHD and RBOHF (Sup Fig. 5c,d). These results are in stark contrast to what has
222 previously been reported, where cell separation during floral abscission was shown to be dependent on
223 RBOHD and RBOHF (Lee et al., 2018). We used a stress transducer to quantify the force needed to
224 remove petals, the petal breakstrength (pBS) (Stenvik et al., 2008), from the receptacle of gradually
225 older flowers along the inflorescence of WT and *rbohd rbohf* flowers. Measurements showed a
226 significant lower pBS value for the *rbohd rbohf* mutant compared to WT at the developmental stage
227 where cell loosening normally occurs, indicating premature cell wall loosening (Sup Fig. 5e).
228 Furthermore, *rbohd rbohf* petals abscised one position earlier than WT (Sup Fig. 5e). In conclusion, we
229 found no RBOHD and RBOHF dependency for cell separation during floral abscission (Crick et al., 2022).
230 Due to a known function of IDA in inducing ROS production (Sup fig 1), these results points towards a
231 role for IDA in modulating additional responses to the process of cell separation.

232

233 *IDA* is upregulated by biotic and abiotic factors

234 In Arabidopsis, infection with the pathogen *P.syringae* induces cauline leaf abscission. Interestingly,
235 stress induced cauline leaf abscission was reduced in plants with mutations in components of the IDA-
236 HAE/HSL2 signaling pathway (Patharkar et al., 2017; Patharkar & Walker, 2016). In addition,
237 upregulation of defense genes in floral AZ cells during the abscission process is altered in the *hae hsl2*
238 mutant (Cai & Lashbrook, 2008; Niederhuth et al., 2013), indicating that the IDA-HAE/HSL2 signaling
239 system may be involved in regulating defense responses in cells undergoing cell separation. To further
240 investigate the involvement of IDA in stress responses we investigated if *IDA* is upregulated by biotic
241 and abiotic elicitors. Transgenic plants containing the *β-glucuronidase (GUS*) gene under the control of
242 the *IDA* promoter (*pIDA:GUS*) have previously been reported to exhibit *GUS* expression in cells
243 overlaying newly formed LR primordia (Butenko et al., 2003; Kumpf et al., 2013). To investigate the
244 expression of the *IDA* gene in response to biotic stress *pIDA:GUS* seedlings were exposed to the bacterial
245 elicitor flg22 and fungal chitin. Compared to the control seedlings, the seedlings exposed to flg22 and
246 chitin showed a significant increase in *GUS* expression in LR primordia (Fig. 3a). Also, when comparing
247 untreated root tips to those exposed to flg22 and chitin we observed a GUS signal in the primary root
248 of flg22 and chitin treated roots (Fig. 3b). We used the fluorogenic substrate 4-methylumbelliferyl β-D-
249 glucuronide (4-MUG) which is hydrolysed to the fluorochrome 4-methyl umbelliferone (4-MU) to
250 quantify GUS-activity (Blazquez, 2007). A significant increase in fluorescence was observed for flg22 and
251 chitin treated samples compared to untreated controls, (Fig. 3b). Exposure of *pIDA:GUS* seedlings to
252 IDAΔN69 did not increase GUS activity in the root, supporting the specific increment of *pIDA:GUS*
253 expression to flg22 peptide (Fig. 3). Spatial *pIDA:GUS* expression was also monitored upon abiotic stress.
254 When *pIDA:GUS* seedling were treated with the osmotic agent mannitol or exposed to salt stress by
255 NaCl, both treatments simulating dry soil, a similar increment in GUS signal was observed surrounding
256 the LR primordia (Fig. 3). However, no *pIDA:GUS* expression was detected in the primary root (Fig. 3b).
257 Taken together these results indicate an upregulation of *IDA* in tissue involved in cell separation
258 processes such as the LR primordia and, interestingly, the root cap upon biotic stress. The process of
259 cell separation is a fast and time-restricted response where cells previously protected by outer cell layers
260 are rapidly exposed to the environment. These cells need strong and rapid protection against the
261 environment, and we therefore aimed to investigate if IDA is involved in modulating immune responses
262 in addition to inducing ROS and $[Ca^{2+}]_{cyt}$ responses.
263

264 mIDA does not induce production of callose as a long term defense response

265 We aimed to investigate a possible role of IDA in regulating long-term defense responses in the plant,
266 such as the production of callose. Callose deposition is a resulting hallmark of the late plant immunity
267 responses that together with other events such as stomatal closure and production of ethylene leads to
268 inhibition of pathogen multiplication and containment of disease (Reviewed in (Wang et al., 2021)).
269 Callose deposition is highly increased in response to flg22 (Gómez-Gómez et al., 1999). We treated WT
270 seedlings with 1 µM mIDA and measured the area of callose deposition in the cotyledons, but detected
271 no difference to water treated controls (Fig. 4a,b). However, flg22 treated WT seedlings showed
272 increased callose deposition, which was not observed in flg22 treated *fls2* seedlings (Fig. 4a,b). These
273 results indicate that mIDA, in contrast to flg22, is not involved in promoting deposition of callose as a
274 long-term defense response.

275

276 mIDA triggers expression of defense-associated marker genes associated with innate immunity.

277 A -well-known part of a plants immune response is the enhanced transcription of genes involved in
278 immunity. Transcriptional reprogramming mostly mediated by WRKY transcription factors takes place
279 during microbe-associated molecular pattern (MAMP)- triggered immunity and is essential to mount an
280 appropriate host defense response (Birkenbihl et al., 2017). We selected well-established defense-
281 associated marker genes: *FLG22-INDUCED RECEPTOR-LIKE KINASE1* (*FRK1*), a specific and early immune-
282 responsive gene activated by multiple MAMPs (Asai et al., 2002; He et al., 2006), *MYB51*, a WRKY target
283 gene, previously shown to increase in response to the MAMP flg22 (Frerigmann et al., 2016) resulting
284 in biosynthesis of the secondary metabolite indolic glucosinolates; and an endogenous danger peptide,
285 ELICITOR PEPTIDE 3 (PEP3) (Huffaker et al., 2006). Seven days-old WT seedlings treated with 1µM mIDA
286 were monitored for changes in transcription of the aforementioned genes by RT-qPCR compared to
287 untreated controls at two time points, 1h and 12h after treatment. All genes showed a significant
288 transcriptional elevation 1 h after mIDA treatment (Fig. 5a). This in accordance with previous reports,
289 where the expression of *FRK1* and *PEP3* was monitored in response to bacterial elicitors (He et al., 2006;
290 Huffaker et al., 2006). After 12 h, *FRK1* and *PEP3* transcription in mIDA treated tissue was not
291 significantly different from untreated tissue; while transcription of MYB51 in mIDA treated tissue
292 remained elevated after 12 h but was significantly lower compared to 1 h after mIDA treatment (Fig.
293 5a). Interestingly, the observed increase in transcription of the defense genes *MYB51* and *PEP3*, was
294 only partially reduced in the *hae hsl2* mutant (Sup Fig. 6). In contrast, *FRK1* showed higher
295 transcriptional levels in the *hae hsl2* mutant compared to WT (Sup Fig. 6). These results indicate that
296 also other receptors than HAE and HSL2 are involved in the mIDA-induced enhancement of the defense
297 genes *FRK1*, *MYB51* and *PEP3*.

298 We then analyzed a plant line expressing nuclear localized YFP from the MYB51 promoter
299 (*pMYB51:YFP*^{N}) (Poncini et al., 2017) treated with mIDA. Enhanced expression of p*MYB51:YFP* was
300 predominantly detected in the meristematic zone of the root after 7 h of mIDA treatment, compared to
301 a non-treated control (Fig. 5b). Moreover, comparison of mIDA induction with the elicitor-triggered
302 response of *pMYB51:YFP*^{N} to flg22 showed similar temporal expression in the root (Sup Fig. 7) .
303 Together, these data show that IDA can trigger a rapid increase in the expression of key genes involved
304 in immunity.

305 We next investigated if the mIDA induced transcription of defense related genes was similar to that
306 induced by flg22. Seven days-old Col-0 WT seedlings were treated for 1h with mIDA, flg22 or a
307 combination of mIDA and flg22 to explore potential additive effects. The relative increase in
308 transcription of the genes tested is similar when seedlings are treated with mIDA and flg22 (Fig. 6).
309 However, when treating seedlings with both peptides the relative transcription of the genes of interest
310 increased substantially. To our surprise, the combined enhanced transcription when seedling where co-
311 treated with both flg22 and mIDA exceeds a simple additive effect of the two peptides, suggesting that
312 IDA has a role in enhancing the defense response triggered by flg22. Based on these results we propose
313 a role for IDA in enhancing immune responses in tissue undergoing cell separation.

314

315 <u>Discussion:</u>

316 Several plant species can abscise infected organs to limit colonization of pathogenic microorganisms
317 thereby adding an additional layer of defense to the innate immune system (Kissoudis et al., 2016;
318 Patharkar et al., 2017). Also, in a developmental context, there is an induction of defense associated
319 genes in AZ cells during cell separation and prior to the formation of the suberized layer that functions
320 as a barrier rendering protection to pathogen attacks (Cai & Lashbrook, 2008; Niederhuth et al., 2013;
321 Roberts et al., 2000; I. Taylor & J. C. Walker, 2018). Interestingly, the induction of defense genes during
322 floral organ abscission is altered in *hae hsl2* plants (Niederhuth et al., 2013). It is largely unknown how
323 molecular components regulating cell separation and how the IDA-HAE/HSL2 signaling pathway,
324 contributes to modulation of plant immune responses. Here we show that the mature IDA peptide,
325 mIDA, is involved in activating known defense responses in Arabidopsis, including the production of ROS,
326 the intracellular release of Ca^{2+} and the transcription of genes known to be involved in defense (Sup Fig.
327 1, Fig. 1, Fig. 2, Fig. 5). We suggest a role for IDA in ensuring optimal cellular responses in tissue
328 undergoing cell separation, regulating both development and defense.

329 The intracellular event occurring downstream of IDA is still partially unknown. Here we report the
330 release of cytosolic Ca^{2+} as a new signaling component. Roots and AZs expressing the Ca^{2+} sensor R-
331 GECO1, showed a $[Ca^{2+}]_{cyt}$ in response to mIDA. Moreover, the increased $[Ca^{2+}]_{cyt}$ in response to mIDA in
332 flowers occurred only at stages where cell separation was taking place, linking the observed $[Ca^{2+}]_{cyt}$
333 response to the temporal point of abscission and the need for an induced local defense response. During
334 floral development the expression of the *HAE* and *HSL2* receptors increase prior to the onset of
335 abscission (Cai & Lashbrook, 2008) and may account for the temporal mIDA induced $[Ca^{2+}]_{cyt}$ response
336 observed.

337 Based on these results, it is likely that the expression of the receptors is the limiting factor for a cell's
338 ability to respond to the mIDA peptide with a $[Ca^{2+}]_{cyt}$ response. However, promoter activity of the
339 receptors are observed in a broader area of the root than the observed $[Ca^{2+}]_{cyt}$ response. As an example,
340 *pHSL2* is found to have a localized activation in the root tip, and when HSL2 is activated by IDL1 be
341 involved in regulation cell separation during root cap sloughing (Shi et al., 2018). IDL1 and IDA have a
342 high degree of similarity in the protein sequence, and *IDL1* expressed under the *IDA* promoter can fully
343 rescue the abscission phenotype observed in the *ida* mutant (Stenvik et al., 2008). We can assume that
344 IDL1 activates similar signaling components in the root cap as those used by IDA. Despite the expression
345 of HSL2 and the involvement of the receptor in root cap sloughing, no $[Ca^{2+}]_{cyt}$ response is observed in
346 this region when plants are treated with the IDA peptide. The absence of an observed $[Ca^{2+}]_{cyt}$ response
347 in the root tip indicates that $[Ca^{2+}]_{cyt}$ is most likely not involved in the cell separation process during root
348 cap sloughing, or that cells involved in this process only are able to induce a $[Ca^{2+}]_{cyt}$ response at a
349 specific developmental time point. Thus, in addition to receptor availability, other factors must be
350 involved in regulating the $[Ca^{2+}]_{cyt}$ response. It is intriguing that the mIDA cellular output is similar to that
351 of flg22 (Kadota et al., 2015; Kadota et al., 2014) yet shows some distinct differences. The spatial
352 distribution of the Ca^{2+} wave originated by mIDA differs from that of flg22. The *rbohd rbohf* mutant
353 shows ROS production in the AZ, indicating that other NADPH oxidases or cell wall peroxidases
354 expressed in the AZ may be involved in ROS production, in contrast to the importance of RBOHD RBOHF
355 in flg22 signaling (Kadota et al., 2015). This suggests that while IDA and flg22 share many components
356 for their signal transduction, such as the BAK1 co-receptor (Chinchilla et al., 2007; X. Meng et al., 2016)
357 and MAPK cascade (Asai et al., 2002; Cho et al., 2008), there are other specific components that are
358 likely important to provide differences in signaling. The difference in callose deposition observed in
359 mIDA and flg22 cotyledons supports this.

360 Interestingly, FLS2 arrangement into nanoscale domains at the PM is dependent on FERONIA (FER). FLS2
361 becomes more disperse and mobile in *fer* mutants, implying a role for FER in regulating FLS2 activity
362 (Gronnier et al., 2022). Also altering of the cell wall affects FLS2 nanoscale organization (McKenna et al.,

363 2019). Formation of nanoscale domains containing the HAE and HSL2 receptors may be an important
364 signaling step in the IDA-HAE/HSL2 signaling pathway. An intriguing thought is a possible co-localization
365 of HAE and HSL2 with FLS2 in nanoscale domains, making a signaling unit possible to involve multiple
366 different receptors responsible for the signaling outcome observed. In this paper, we show that co-
367 treatment with mIDA and flg22 induces an enhanced transcription of defense related genes. How FLS2,
368 HAE and HSL2 communicate at the plasma membrane of the responsive cells may give the answers to
369 the molecular mechanisms behind the augmented transcriptional regulation observed when co-
370 treatment of IDA and flg22 is performed (Fig. 6). We can investigate possible interaction partners of
371 HAE and HSL2 looking at available data from a sensitized high-throughput interaction assay between
372 extracellular domains (ECDs) of 200 Leucine Rich Repeat (LRR) (Smakowska-Luzan et al., 2018).
373 Interestingly, LRR-RLKs known to play a function in biotic or abiotic stress responses, such as RECEPTOR-
374 LIKE KINASE7 (RLK7), STRUBBELIG-RECEPTOR FAMILY3 , RECEPTOR-LIKE PROTEIN KINASE 1 and FRK1,
375 are found to interact mainly with HSL2, whereas HAE shows interaction with LRRs mainly involved in
376 development (Sup Fig. 8). RLK7 has recently been identified as an additional receptor for CEP4, involved
377 in regulating cell surface immunity and response to nitrogen starvation, indication a role of RLK7 as an
378 additional receptor regulating defense responses in known peptide-receptor complexes (Rzemieniewski
379 et al., 2022). It would be interesting to investigate a possible role of RLK7 in IDA-HAE/HSL2 signaling as
380 a possible signaling partner in the observed IDA-induced early defense responses.

381

382 In this paper, we propose a model where the IDA-HAE/HSL2 signaling pathway modulates defense
383 responses in tissues undergoing cell separation. It is beneficial for the plant to ensure an upregulation
384 of defense responses in tissues undergoing cell separation as a precaution against pathogen attack. This
385 tissue is a major entry route for pathogens, and by combining the need of both the IDA peptide and the
386 pathogen molecular pattern, such as flg22, for the induction of a strong defense response, the plant
387 ensures maximum immunity in the most prone cells without spending energy inducing this in all cells
388 (Fig. 7). Such a molecular mechanism, where the presence of mIDA in tissue exposed to stress leads to
389 maximum activation of the immune responses, will ensure maximal protection of infected cells during
390 cell separation, cells which are major potential entry routes for invading pathogens.

391 Movies

392 **Movie 1:** $[Ca^{2+}]_{cyt}$ dynamics in R-GECO1 expressing root tip in response to 1 µM mIDA. 10 days-old roots
393 were treated with 1 µM mIDA and changes in $[Ca^{2+}]_{cyt}$ was recorded over time. Response shown as
394 normalized fluorescence intensities (ΔF/F). Images were recorded with a frame rate of 5 seconds. Movie

395 corresponds to measurements shown in Fig. 1a. Representative response from 10 roots. Time shown as,
396 hh:mm:ss.
397
398 **Movie 2:** $[Ca^{2+}]_{cyt}$ dynamics in R-GECO1 expressing root tip in response to 1 µM flg22 10 days-old roots were
399 treated with 1 µM flg22 and changes in $[Ca^{2+}]_{cyt}$ was recorded over time. Response shown as normalized
400 fluorescence intensities (ΔF/F). Images were recorded with a frame rate of 5 seconds. Movie corresponds
401 to measurements shown in Fig. 1b. Representative response from 10 roots. Time shown as, hh:mm:ss.
402
403 **Movie 3:** $[Ca^{2+}]_{cyt}$ dynamics in R-GECO1 expressing AZ in response to 1 µM mIDA. Flowers at position 6 were
404 treated with 1 µM mIDA and changes in $[Ca^{2+}]_{cyt}$ was recorded over time. Response shown as normalized
405 fluorescence intensities (ΔF/F). Images were recorded with a frame rate of 5 seconds. Movie corresponds
406 to measurements shown in Fig. 2a. Representative response from 10 flowers. Time shown as, hh:mm:ss.
407
408 **Sup Movie 1:** $[Ca^{2+}]_{cyt}$ dynamics in R-GECO1 expressing root tip in response to 1 mM eATP. 1 mM eATP will
409 induce a strong increase in $[Ca^{2+}]_{cyt}$ and was added as a last treatment to all roots acting as a positive control.
410 Response shown as normalized fluorescence intensities (ΔF/F). Images were recorded with a frame rate of
411 5 seconds. Movie corresponds to measurements shown in Fig. 1a. Representative response from 10 roots.
412 Time shown as, hh:mm:ss.
413
414 **Sup Movie 2:** $[Ca^{2+}]_{cyt}$ dynamics in R-GECO1 expressing AZ in response to to 1 µM of the inactive IDA peptide,
415 $IDA^{\Delta N69}$. Flowers at position 6 were treated with 1 µM $IDA^{\Delta N69}$ and changes in $[Ca^{2+}]_{cyt}$ was recorded over
416 time. Response shown as normalized fluorescence intensities (ΔF/F). Images were recorded with a frame
417 rate of 5 seconds. Movie corresponds to measurements shown in Sup Fig. 3. Representative response from
418 10 flowers. Time shown as, hh:mm:ss.
419
420
421
422 ***Methods***

423 Accession numbers of genes studied in this work:

424 HSL2 At5g65710, IDA At1g68765, FLS2 At5g46330, HAE At4g28490, MYB51 At1g18570, RBOHD
425 At5g47910, RBOHF At1g64060, PEP3 At5g64905, WRKY33 At2g38470, FRK1 At2g19190. Plant lines used
426 in this work: Ecotype Colombia-0 (Col-0) was used as wild type (WT). Mutant line: *hae* (SALK_021905),
427 *hsl2*, (SALK_030520), *fls2* (SALK_062054), *rbohd* (SALK_070610), *rbohf* (SALK_059888), *cngc1*

428 (SAIL_443), *cngc2* (SALK_066908), *cngc4* (SALK_081369), *cngc5* (SALK_149893), *cngc6* (SALK_064702),
429 *cngc9* (SAIL_736), *cngc12* (SALK_093622). SALK lines were provided from Nottingham Arabidopsis Stock
430 Centre (NASC).

431 Plant lines

432 The pIDA:GUS, pHSL2:Venus-H2B and pMYB51:YFPN lines have been described previously (Kumpf et al.,
433 2013; Poncini et al., 2017; Shi et al., 2018).The promoters of HAE (1601 bp (Kumpf et al., 2013) and HSL2
434 (2300 bp (Sto et al., 2015))were available in the pDONRZeo vector (Thermo Fischer Scientific).
435 Sequences corresponding to the FLS2 promoter (988 bp (Robatzek et al., 2006)) were amplified from
436 WT DNA (primers are listed in table 2) and cloned into the pDONRZeo vector (Thermo Fischer Scientific).
437 All promoter constructs were further recombined into the promotor:Venus (YFP)-H2B and
438 Cerulean(CFP)-H2B destination vectors (Somssich et al., 2016) using the Invitrogen Gateway cloning
439 system (Thermo Fischer Scientific). Constructs were transformed into *Agrobacterium tumefaciens*
440 (A.tumefaciens) C58 and the floral dip method (Clough & Bent, 1998) was used to generate transgenic
441 lines. Single-copy homozygous plant lines were selected and used in this study. The CDS of HAE was
442 cloned into the pEarleyGate101 destination vector (Earley et al., 2006) using the Invitrogen Gateway
443 cloning system and transformed into A.tumefaciens C58 and further used to generate the 35S:HAE:YFP
444 lines.

445 Growth conditions

446 Plants were grown in long day conditions (8h dark and 16h light) at 22°C. Seeds were surface sterilized
447 and plated out on MS-2 plates, stratified for 24 h at 4 °C and grown on plates for 7 days before
448 transferred to soil.

449 Peptide sequences

450 Peptides used in this study were ordered from BIOMATIK. Peptide sequences are listed in
451 Supplementary Table 1.

452 Primers

453 Primers for genotyping and generation of constructs were generated using VectorNTI. Gene specific
454 primers for RT-qPCR were generated using Roche Probe Library Primer Design. All primers are listed in
455 Supplementary Table 2.

456 Histochemical GUS assay

457 Seven days-old seedlings were pre-incubated for 12 h in liquid MS-2 medium containing stimuli of
458 interest; 1 µM peptide (table 1), 60 mM Mannitol (M4125 – Sigma), 20 µg/mL Chitin (C9752 – Sigma),
459 50 mM NaCl and then stained for GUS activity following the protocol previously described (Stenvik et
460 al., 2008). Roots were pictured using a Zeiss Axioplan2 microscope with an AxioCam HRc, 20x air
461 objective. The assay was performed on 10 individual roots and the experiment was repeated 3 times.

462 Fluorescent GUS assay

463 Seven days-old seedlings were pre-incubated for 12 h in liquid MS-2 medium with or without stimuli of
464 interest; 1 µM peptide (table 1), 60 mM Mannitol (M4125 – Sigma), 20 µg/mL Chitin (C9752 – Sigma),
465 50 mM NaCl. After treatment, 10 seedlings were incubated in wells containing 1 mL reaction mix
466 described in (Blazquez, 2007) containingcontaining: 10 mM EDTA (pH 8.0), 0,1 % SDS, 50 mM Sodium
467 Phosphate (pH 7.0), 0,1 % Triton X-100, 1 mM 4-MUG (, M9130-Sigma) and incubated at 37 °C for 6 h.
468 Six 100 µl aliquots from each well were transferred to individual wells in a microtiter plate and the
469 reaction was stopped by adding 50 µl of stop reagent (1 M Sodium Carbonate) to each well.
470 Fluorescence was detected by the use of a Wallac 1420 VICTOR2 microplate luminometer (PerkinElmer)
471 using an excitation wavelength of 365 nm and a filter wavelength of 430 nm. Each experiment was
472 repeated 3 times.

473 Confocal laser microscopy of roots and flowers expressing promoter:Venus/YFP-H2B and promoter:
474 Cerulean-H2B construct

475 Imaging of 7 days-old roots was performed on a LSM 880 Airyscan confocal microscope equipped with
476 two flanking PMTs and a central 32 array GaAsP detector. Images were acquired with Zeiss Plan-
477 Apochromat 20x/0.8 WD=0.55 M27 objective and excited with laser light of 405 nm, 488 nm and 561
478 nm. Roots were stained by 1 µM propidium iodide for 10 min and washed in dH_2O before imaging.
479 Imaging of flowers was performed on an Andor Dragonfly spinning disk confocal using an EMCCD iXon
480 Ultra detector. Images were acquired with a 10x plan Apo NA 0,45 dry objective and excited with laser
481 light of 405 nm, 488 nm and 561 nm. Maximum intensity projections of z-stacks were acquired with
482 step size of 1,47 µm. Image processing was performed in FIJI 51. These steps are: background
483 subtraction, gaussian blur/smooth, brightness/contrast. Imaging was performed at the NorMIC Imaging
484 platform.

485

486 Calcium imaging using the R-GECO1 sensor

487 $[Ca^{2+}]_{cyt}$ in roots were detected using WT plants expressing the cytosolic localized single-fluorophore
488 based Ca^{2+} sensor, R-GECO1 (Keinath et al., 2015). Measurements were performed using a confocal
489 laser scanning microscopy Leica TCS SP8 STED 3X using a 20x multi NA 0.75 objective. Images were
490 recorded with a frame rate of 5 seconds at 400 Hz. Seedling mounting was performed as described in
491 (Krebs & Schumacher, 2013). The plant tissues were incubated overnight in half strength MS, 21°C and
492 continuous light conditions before the day of imaging. $[Ca^{2+}]_{cyt}$ in the abscission zone were detected
493 using WT plants expressing R-GECO1 (Keinath et al., 2015). Abscission zones of position 7 were used.
494 Mounting of the abscission zones were performed using the same device as for seedlings (Krebs &
495 Schumacher, 2013). The abscission zones were incubated in half strength MS medium for 1 h before
496 imaging. Measurements were performed with a Zeiss LSM880 Airyscan using a Plan-Apochromat 10×
497 air NA 0.30 objective. Images were recorded with a frame rate of 10 seconds. R-GECO1 was excited
498 with a white light laser at 561 nm and its emission was detected at 590 nm to 670 nm using a HyD
499 detector. Laser power and gain settings were chosen for each experiment to maintain comparable
500 intensity values. For mIDA and flg22 two-fold concentrations were prepared in half strength MS. mIDA
501 or flg22 were added in a 1:1 volume ratio to the imaging chamber (final concentration 1 µM). ATP was
502 prepared in a 100-fold concentration in half strength MS and added as a last treatment in a 1:100
503 volume ratio (final concentration 1 mM) to the imaging chamber as a positive control for activity of the
504 R-GECO1 sensor (Movie 3). Image processing was performed in FIJI. These steps are: background
505 subtraction, gaussian blur, MultiStackReg v1.45 (http://bradbusse.net/sciencedownloads.html), 32-bit
506 conversion, threshold. Royal was used as a look up table. Fluorescence intensities of indicated ROIs were
507 obtained from the 32-bit images (Krebs & Schumacher, 2013). Normalization was done using the
508 following formula $\Delta F/F = (F-F0)/F0$ where F0 represents the mean of at least 1 min measurement
509 without any treatment. R-GECO1 measurements were performed at the Center for Advanced imaging
510 (CAi) at HHU and at NorMIC Imaging platform at the University of Oslo.

511 <u>Calcium measurements using the Aequorin (pMAQ2) sensor</u>

512 $[Ca^{2+}]_{cyt}$ in seedlings and flowers were detected using WT plants expressing p35S-apoaequorin (pMAQ2)
513 located to cytosol (Aeq) (Knight et al., 1991; Ranf et al., 2011). Aequorin luminescence was measured
514 as previously described (Ranf et al., 2012). Emitted light was detected by the use of a Wallac 1420
515 VICTOR2 microplate luminometer (PerkinElmer). Differences in Aeq expression levels due to seedling
516 size and expression of sensor were corrected by using luminescence at specific time point (L)/Max
517 Luminescence (Lmax). Lmax was measured after peptide treatment by individually adding 100 µL 2 M
518 $CaCl_2$ to each well and measuring luminescence constantly for 180 seconds (Ranf et al., 2012). 2 M $CaCl_2$
519 disrupts the cells and releases the Aeq sensor into the solution where it will react with Ca^{2+} and release
520 the total possible response in the sample (Lmax) in form of a luminescent peak. A final concentration of

521 1 µM mIDA was added to each wells at the start of measurements. For inhibitor treatements, Aeq-
522 seedlings were incubated in in 2mM EGTA (Sigma-Aldrich) or 1mM $LaCL_3$ (Sigma-Aldrich) O/N before
523 measurements. For seedlings 3 independent experiments were performed with 12 replications in each
524 experiment. For flowers 3 independent experiments were performed with 4-6 replications in each
525 experiment.

526 Measurements of reactive oxygen species (ROS)

527 ROS production was monitored by the use of a luminol-dependent assay as previously described
528 (Butenko et al., 2014) using a Wallac 1420 VICTOR2 microplate luminometer (PerkinElmer). Arabidopsis
529 leaves expressing *35S:HAE:YFP* were cut into leaf discs and incubated in water overnight before
530 measurements. A final concentration of 1 µM mIDA was added to each well at the start of
531 measurements. All measurements were performed on 6 leaf discs and each experiment was repeated
532 3 times.

533 ROS stain (H2DCF-DA)

534 Flowers at position 6 were gently incubated in staining solution (25 µM (2',7'-dichlorodihydrofluorescein
535 diacetate) (H2DCF-DA) (Sigma-Aldrich, D6883), 50 mM KCL, 10 mM MES) for 10 min and further washed
536 3 times in wash solution (50 mM KCL, 10 mM MES). For the *hae hsl2* mutant the floral organs were
537 forcibly removed immediately before imaging. Imaging was done using a Dragonfly Airy scan spinning
538 disk confocal microscope, excited by a 488 nm laser. A total of 9 flowers per genotype were imaged.
539 The experiment was repeated 2 independent times.

540 Callose deposition staining and quantification

541 Callose deposition experiments were conducted as per (Luna et al., 2011) with modifications. Seeds
542 from WT and *fls2* were vapor-phase sterilized for 4 h. Seeds were transferred to 12-well plates
543 containing 1 mL of filter-sterilized MS medium and 0. 5 % MES with a final pH of 5.7, and stratified in
544 the dark at 4 °C for 2 days. Plates were consecutively transferred to a growth chamber with 16 h of light
545 (150µE m-2 s-1)/8h darkness cycle at 22°C. On the seventh day, growth medium was refreshed under
546 sterile conditions. On the eight day the treatments were applied: addition of 10 µL of water (mock); 10
547 µL of 100 µM flg22; or 10 µL of 100 µM mIDA (final peptide concentrations of 1 µM). After 24 h the
548 growth medium was replaced with 9 5% ethanol and incubated overnight. Ethanol was replaced with
549 an 8 M NaOH softening solution and incubated for 2 h. Seedlings were washed 3 times in water and
550 immediately transferred to the aniline blue staining solution (100 mM KPO4-KOH, pH 11; 0.1 % aniline
551 blue). After 2 h of staining, the seedlings were mounted on 50 % glycerol and imaged under a ZEISS
552 epifluorescence microscope with UV filter (BP 365/12 nm; FT 395 nm; LP 397 nm). Image analysis was

553 performed on FIJI (Schindelin et al., 2012). In brief, cotyledons were cropped and measured the leaf
554 area. Images were thresholded to remove autofluorescence and area of depositions measured to
555 calculate the ratio of callose deposition area per cotyledon area unit. Between 9-12 seedlings were
556 analyzed per genotype x treatment combination.

557 Real time quantitative PCR (RT-qPCR)

558 Seven days-old Arabidopsis seedlings (WT, *hae hsl2*) grown vertically on ½ sucrose MS-2 plates were
559 transferred to liquid ½ MS-2 medium (non-treated) and liquid ½ MS-2 medium containing 1 µM peptide
560 and incubated in growth chambers for 1 h or 12 h. Seedlings were flash-frozen in liquid nitrogen before
561 total RNA was extracted using SpectrumTM Plant Total RNA Kit (SIGMA Aldrich). cDNA synthesis was
562 performed as previously described (Grini et al., 2009). RT-qPCR was performed according to protocols
563 provided by the manufacturer using FastStart Essential DNA Green Master (Roche) and LightCycler96
564 (Roche) instrument. ACTIN2 was used to normalize mRNA levels as described in (Grini et al., 2009). Three
565 biological replicates and 4 technical replicates including standard curves were performed for each
566 sample.

567 Petal Break strength (pBS)

568 The force required to remove a petal at a given position on the inflorescence was measured in gram
569 equivalents using a load transducer as previously described (Stenvik et al., 2008). Plants were grown
570 until they had at least 15 positions on the inflorescence. A minimum of 15 petals per position were
571 measured. pBS measurements were performed on WT, *rbohd rbohf* (SALK_070610 SALK_059888) and
572 *hae hsl2* (SALK_021905 SALK_030520) plants.

573 Statistical methods

574 Two tailed students t-test ($p < 0.05$) was used to identify significant differences in the fluorescent GUS
575 assay by comparing treated samples to untreated samples of the same plant line. Statistical analysis of
576 the RT-qPCR results was performed on all replicas using ONE-WAY or TWO-WAY ANOVA (as stated in
577 the figure text) and post-hoc Tukey's test ($p < 0.05$). Two tailed students t-test with ($p < 0.05$) was used
578 in the petal break strength (pBS) measurements to identify significant differences from WT at a given
579 position on the inflorescence.

580

581 Acknowledgements
582 We thank M.K. Anker, I.M. Stø, V. Iversen and R. Falleth for technical assistance in the laboratory and
583 phytotrone. We thank the NorMic Imaging platform for the use and technical support. This work was

supported by the Research Council of Norway (grant 230849) to V.O. and M.A.B. Work by R. Simon and and M.B. was supported through CEPLAS.

Author contributions

V.O. generated Arabidopsis lines and constructs, tested IDA expression to biotic and abiotic stress, performed gene expression studies, phenotypic analysis of mutants and ROS measurements. V.O. and M.B. performed Ca^{2+} measurements S.G-T. performed the callose deposition assays. V.O., S. G-T., M.B., R.Simon and M.A.B designed experiments, analyzed data, and drafted the manuscript. V.O. and M.A.B wrote the paper with input from all authors.

Competing interests

The authors have no competing interests.

Materials and correspondence

Correspondence to Melinka A. Butenko, m.a.butenko@ibv.uio.no

Supplementary Tables

Supplementary Table 1: Peptide sequences

Peptide	Amino acid sequence
mIDA	PIPPSAoSKRHN
flg22	QRLSTGSRINSAKDDAAGLQIA
IDA$^{\Delta N69}$	PIPPSAoSKRH

(o = hydroxyproline)

Supplementary Table 2: Primers sequences and function

Function	Primer name	Primer sequence 5’-3’
Cloning promoter FLS2	PromFLS2 -988bp Attb1	5’GGGGACAAGTTTGTACAAAAAAGCAGGCTTA GAAGTTGTGAATTGTGAT’3
Cloning promoter FLS2	PromFLS2 -988bp Attb2	5’GGGGACCACTTTGTACAAGAAAGCTGGGTA GGTTTAGACTTTAGAAGA’3
Genotype hsl2	Hsl2 LP	5’CGTCTTGAGCTAGCCAACAAC’3
Genotype hsl2	Hsl2 RP	5’GTCCAATCAAGTGGAGAAACG’3
Genotype hae	Haesa LP	5’CACCTTCCTTCTCTCCATTCC’3
Genotype hae	Haesa RP	5’GTTCGAGAAGTGACAAGCGAG’3
Genotype SALK-lines	Lbb1-	5’GCGTGGACCGCTTGCTGCAACT’3
Genotype rbohd SALK_070610C	LP_SALK_070610C	5’TTTCAACGCCTTTTGGTACAC’3
Genotype rbohd SALK_070610C	RP_SALK_070610C	5’GTTACCTATTCTTTTGCCGGG’3
Genotype rbohf SALK_059888	LP_SALK_059888	5’CAAAGAGCTCTTCGTGGTTTG’3
Genotype rbohf SALK_059888	RP_SALK_059888	5’TCTCTATTGTATCTTGTGTCACCG’3
Genotype fls2 SALK_062054	FLS2_SALK_062054 Fw	5’GGTTCGATTCCTTCTGGAATC’3
Genotype fls2 SALK_062054	FLS2_SALK_062054 Rv	5’CCTGAGTTTTTGAAGCTTCCC’3
qPCR	33.FRK1 Fw	5’AACTTAGGAGACTATTTGGCAGGTAA’3
qPCR	33.FRK1 Rv	5’TGCATCTAATGATATCTTCAACCTCT’3
qPCR	63.PEP3 Fw	5’GCGAGGAAGATGAGAGTATCG’3
qPCR	63.PEP3 Rv	5’TCAATGGTCATGCCATCTTCT’3
qPCR	91.MYB51 Fw	5’GGCCAATTATCTTAGACCTGACA’3
qPCR	91.MYB51 Rv	5’CCACGAGCTATAGCAGACCATT’3
qPCR reference gene	act2int2 sense	5’CCCTGAGGAGCACCCAGTTCTACTC’3

qPCR reference gene	act2int2 antisense	5'CCGCAAGATCAAGACGAAGGATAGC'3

605

606

607

608 References:

609 Agustí, J., Merelo, P., Cercós, M., Tadeo, F. R., & Talón, M. (2009). Comparative transcriptional survey
610 between laser-microdissected cells from laminar abscission zone and petiolar cortical tissue
611 during ethylene-promoted abscission in citrus leaves. *BMC Plant Biology*, *9*(1), 127.
612 https://doi.org/10.1186/1471-2229-9-127
613 Asai, T., Tena, G., Plotnikova, J., Willmann, M. R., Chiu, W. L., Gomez-Gomez, L., Boller, T., Ausubel, F.
614 M., & Sheen, J. (2002). MAP kinase signalling cascade in Arabidopsis innate immunity. *Nature*,
615 *415*(6875), 977-983. https://doi.org/10.1038/415977a
616 Birkenbihl, R. P., Kracher, B., & Somssich, I. E. (2017). Induced Genome-Wide Binding of Three
617 Arabidopsis WRKY Transcription Factors during Early MAMP-Triggered Immunity. *Plant Cell*,
618 *29*(1), 20-38. https://doi.org/10.1105/tpc.16.00681
619 Blazquez, M. (2007). Quantitative GUS Activity Assay in Intact Plant Tissue. *CSH Protoc*, *2007*,
620 pdb.prot4688. https://doi.org/10.1101/pdb.prot4688
621 Bleecker, A. B., & Patterson, S. E. (1997). Last exit: senescence, abscission, and meristem arrest in
622 Arabidopsis. *Plant Cell*, *9*(7), 1169-1179. https://doi.org/10.1105/tpc.9.7.1169
623 Breiden, M., Olsson, V., Blümke, P., Schlegel, J., Gustavo-Pinto, K., Dietrich, P., Butenko, M. A., & Simon,
624 R. (2021). The Cell Fate Controlling CLE40 Peptide Requires CNGCs to Trigger Highly Localized
625 Ca2+ Transients in Arabidopsis thaliana Root Meristems. *Plant Cell Physiol*, *62*(8), 1290-1301.
626 https://doi.org/10.1093/pcp/pcab079
627 Butenko, M. A., Patterson, S. E., Grini, P. E., Stenvik, G.-E., Amundsen, S. S., Mandal, A., & Aalen, R. B.
628 (2003). *INFLORESCENCE DEFICIENT IN ABSCISSION* Controls Floral Organ Abscission in
629 Arabidopsis and Identifies a Novel Family of Putative Ligands in Plants. *Plant Cell*, *15*, 2296-
630 2307.
631 Butenko, M. A., Wildhagen, M., Albert, M., Jehle, A., Kalbacher, H., Aalen, R. B., & Felix, G. (2014). Tools
632 and Strategies to Match Peptide-Ligand Receptor Pairs. *Plant Cell*, *26*(5), 1838-1847.
633 https://doi.org/10.1105/tpc.113.120071
634 Cai, S., & Lashbrook, C. C. (2008). Stamen abscission zone transcriptome profiling reveals new
635 candidates for abscission control: enhanced retention of floral organs in transgenic plants
636 overexpressing Arabidopsis ZINC FINGER PROTEIN2. *Plant Physiol*, *146*(3), 1305-1321.
637 https://doi.org/10.1104/pp.107.110908
638 Castro, B., Citterico, M., Kimura, S., Stevens, D. M., Wrzaczek, M., & Coaker, G. (2021). Stress-induced
639 reactive oxygen species compartmentalization, perception and signalling. *Nat Plants*, *7*(4),
640 403-412. https://doi.org/10.1038/s41477-021-00887-0
641 Chinchilla, D., Zipfel, C., Robatzek, S., Kemmerling, B., Nurnberger, T., Jones, J. D., Felix, G., & Boller, T.
642 (2007). A flagellin-induced complex of the receptor FLS2 and BAK1 initiates plant defence.
643 *Nature*, *448*(7152), 497-500. https://doi.org/10.1038/nature05999
644 Cho, S. K., Larue, C. T., Chevalier, D., Wang, H., Jinn, T. L., & Zhang, S. (2008). Regulation of floral organ
645 abscission in Arabidopsis thaliana. *Proc Natl Acad Sci USA.*, *105*.
646 https://doi.org/10.1073/pnas.0805539105
647 Clough, S. J., & Bent, A. F. (1998). Floral dip: a simplified method for Agrobacterium-mediated
648 transformation of Arabidopsis thaliana. *The Plant Journal*, *16*(6), 735-743.

Crick, J., Corrigan, L., Belcram, K., Khan, M., Dawson, J. W., Adroher, B., Li, S., Hepworth, S. R., & Pautot, V. (2022). Floral organ abscission in Arabidopsis requires the combined activities of three TALE homeodomain transcription factors. *J Exp Bot*, *73*(18), 6150-6169. https://doi.org/10.1093/jxb/erac255

Dubiella, U., Seybold, H., Durian, G., Komander, E., Lassig, R., Witte, C. P., Schulze, W. X., & Romeis, T. (2013). Calcium-dependent protein kinase/NADPH oxidase activation circuit is required for rapid defense signal propagation. *Proc Natl Acad Sci U S A*, *110*(21), 8744-8749. https://doi.org/10.1073/pnas.1221294110

Earley, K. W., Haag, J. R., Pontes, O., Opper, K., Juehne, T., Song, K., & Pikaard, C. S. (2006). Gateway-compatible vectors for plant functional genomics and proteomics. *Plant J*, *45*(4), 616-629. https://doi.org/10.1111/j.1365-313X.2005.02617.x

Felix, G., Duran, J. D., Volko, S., & Boller, T. (1999). Plants have a sensitive perception system for the most conserved domain of bacterial flagellin. *The Plant Journal*, *18*(3), 265-276. https://onlinelibrary.wiley.com/doi/full/10.1046/j.1365-313X.1999.00265.x?sid=nlm%3Apubmed

Frerigmann, H., Pislewska-Bednarek, M., Sanchez-Vallet, A., Molina, A., Glawischnig, E., Gigolashvili, T., & Bednarek, P. (2016). Regulation of Pathogen-Triggered Tryptophan Metabolism in Arabidopsis thaliana by MYB Transcription Factors and Indole Glucosinolate Conversion Products. *Mol Plant*, *9*(5), 682-695. https://doi.org/10.1016/j.molp.2016.01.006

Geiger, D., Scherzer, S., Mumm, P., Marten, I., Ache, P., Matschi, S., Liese, A., Wellmann, C., Al-Rasheid, K., & Grill, E. (2010). Guard cell anion channel SLAC1 is regulated by CDPK protein kinases with distinct Ca2+ affinities. *Proceedings of the National Academy of Sciences*, *107*(17), 8023-8028.

Gómez-Gómez, L., Felix, G., & Boller, T. (1999). A single locus determines sensitivity to bacterial flagellin in Arabidopsis thaliana. *Plant J*, *18*(3), 277-284. https://doi.org/10.1046/j.1365-313x.1999.00451.x

Grini, P. E., Thorstensen, T., Alm, V., Vizcay-Barrena, G., Windju, S. S., Jorstad, T. S., Wilson, Z. A., & Aalen, R. B. (2009). The ASH1 HOMOLOG 2 (ASHH2) histone H3 methyltransferase is required for ovule and anther development in Arabidopsis. *PLoS One*, *4*(11), e7817. https://doi.org/10.1371/journal.pone.0007817

Gronnier, J., Franck, C. M., Stegmann, M., DeFalco, T. A., Abarca, A., von Arx, M., Dünser, K., Lin, W., Yang, Z., Kleine-Vehn, J., Ringli, C., & Zipfel, C. (2022). Regulation of immune receptor kinase plasma membrane nanoscale organization by a plant peptide hormone and its receptors. *Elife*, *11*. https://doi.org/10.7554/eLife.74162

He, P., Shan, L., Lin, N. C., Martin, G. B., Kemmerling, B., Nurnberger, T., & Sheen, J. (2006). Specific bacterial suppressors of MAMP signaling upstream of MAPKKK in Arabidopsis innate immunity. *Cell*, *125*(3), 563-575. https://doi.org/10.1016/j.cell.2006.02.047

Huffaker, A., Pearce, G., & Ryan, C. A. (2006). An endogenous peptide signal in Arabidopsis activates components of the innate immune response. *Proc Natl Acad Sci U S A*, *103*(26), 10098-10103. https://doi.org/10.1073/pnas.0603727103

Kadota, Y., Shirasu, K., & Zipfel, C. (2015). Regulation of the NADPH Oxidase RBOHD During Plant Immunity. *Plant and Cell Physiology*, *56*(8), 1472-1480. https://doi.org/10.1093/pcp/pcv063

Kadota, Y., Sklenar, J., Derbyshire, P., Stransfeld, L., Asai, S., Ntoukakis, V., Jones, J. D., Shirasu, K., Menke, F., Jones, A., & Zipfel, C. (2014). Direct regulation of the NADPH oxidase RBOHD by the PRR-associated kinase BIK1 during plant immunity. *Mol Cell*, *54*(1), 43-55. https://doi.org/10.1016/j.molcel.2014.02.021

Keinath, N. F., Waadt, R., Brugman, R., Schroeder, J. I., Grossmann, G., Schumacher, K., & Krebs, M. (2015). Live Cell Imaging with R-GECO1 Sheds Light on flg22- and Chitin-Induced Transient [Ca(2+)]cyt Patterns in Arabidopsis. *Mol Plant*, *8*(8), 1188-1200. https://doi.org/10.1016/j.molp.2015.05.006

Kissoudis, C., Sunarti, S., van de Wiel, C., Visser, R. G., van der Linden, C. G., & Bai, Y. (2016). Responses to combined abiotic and biotic stress in tomato are governed by stress intensity and resistance mechanism. *J Exp Bot*, *67*(17), 5119-5132. https://doi.org/10.1093/jxb/erw285

Knight, H., Trewavas, A. J., & Knight, M. R. (1997). Calcium signalling in Arabidopsis thaliana responding to drought and salinity. *Plant J*, *12*(5), 1067-1078. https://doi.org/10.1046/j.1365-313x.1997.12051067.x

Knight, M. R., Campbell, A. K., Smith, S. M., & Trewavas, A. J. (1991). Transgenic plant aequorin reports the effects of touch and cold-shock and elicitors on cytoplasmic calcium. *Nature*, *352*(6335), 524-526. https://doi.org/10.1038/352524a0

Krebs, M., & Schumacher, K. (2013). Live cell imaging of cytoplasmic and nuclear Ca2+ dynamics in Arabidopsis roots. *Cold Spring Harbor Protocols*, *2013*(8), pdb. prot073031.

Kudla, J., Becker, D., Grill, E., Hedrich, R., Hippler, M., Kummer, U., Parniske, M., Romeis, T., & Schumacher, K. (2018). Advances and current challenges in calcium signaling. *New Phytol*, *218*(2), 414-431. https://doi.org/10.1111/nph.14966

Kumpf, R. P., Shi, C. L., Larrieu, A., Sto, I. M., Butenko, M. A., Peret, B., Riiser, E. S., Bennett, M. J., & Aalen, R. B. (2013). Floral organ abscission peptide IDA and its HAE/HSL2 receptors control cell separation during lateral root emergence. *Proc Natl Acad Sci U S A*, *110*(13), 5235-5240. https://doi.org/10.1073/pnas.1210835110

Kärkönen, A., & Kuchitsu, K. (2015). Reactive oxygen species in cell wall metabolism and development in plants. *Phytochemistry*, *112*, 22-32. https://doi.org/https://doi.org/10.1016/j.phytochem.2014.09.016

Ladwig, F., Dahlke, R. I., Stuhrwohldt, N., Hartmann, J., Harter, K., & Sauter, M. (2015). Phytosulfokine Regulates Growth in Arabidopsis through a Response Module at the Plasma Membrane That Includes CYCLIC NUCLEOTIDE-GATED CHANNEL17, H+-ATPase, and BAK1. *Plant Cell*, *27*(6), 1718-1729. https://doi.org/10.1105/tpc.15.00306

Lee, Y., Yoon, T. H., Lee, J., Jeon, S. Y., Lee, J. H., Lee, M. K., Chen, H., Yun, J., Oh, S. Y., Wen, X., Cho, H. K., Mang, H., & Kwak, J. M. (2018). A Lignin Molecular Brace Controls Precision Processing of Cell Walls Critical for Surface Integrity in Arabidopsis. *Cell*, *173*(6), 1468-1480.e1469. https://doi.org/10.1016/j.cell.2018.03.060

Li, L., Li, M., Yu, L., Zhou, Z., Liang, X., Liu, Z., Cai, G., Gao, L., Zhang, X., Wang, Y., Chen, S., & Zhou, J. M. (2014). The FLS2-associated kinase BIK1 directly phosphorylates the NADPH oxidase RbohD to control plant immunity. *Cell Host Microbe*, *15*(3), 329-338. https://doi.org/10.1016/j.chom.2014.02.009

Luna, E., Pastor, V., Robert, J., Flors, V., Mauch-Mani, B., & Ton, J. (2011). Callose deposition: a multifaceted plant defense response. *Mol Plant Microbe Interact*, *24*(2), 183-193. https://doi.org/10.1094/mpmi-07-10-0149

Ma, Y., Walker, R. K., Zhao, Y., & Berkowitz, G. A. (2012). Linking ligand perception by PEPR pattern recognition receptors to cytosolic Ca2+ elevation and downstream immune signaling in plants. *Proc Natl Acad Sci U S A*, *109*(48), 19852-19857. https://doi.org/10.1073/pnas.1205448109

Matsubayashi, Y. (2011). Post-translational modifications in secreted peptide hormones in plants. *Plant Cell Physiol*, *52*(1), 5-13. https://doi.org/10.1093/pcp/pcq169

McKenna, J. F., Rolfe, D. J., Webb, S. E. D., Tolmie, A. F., Botchway, S. W., Martin-Fernandez, M. L., Hawes, C., & Runions, J. (2019). The cell wall regulates dynamics and size of plasma-membrane nanodomains in Arabidopsis. *Proc Natl Acad Sci U S A*, *116*(26), 12857-12862. https://doi.org/10.1073/pnas.1819077116

Meng, X., Zhou, J., Tang, J., Li, B., de Oliveira, M. V., Chai, J., He, P., & Shan, L. (2016). Ligand-Induced Receptor-like Kinase Complex Regulates Floral Organ Abscission in Arabidopsis. *Cell Rep*, *14*(6), 1330-1338. https://doi.org/10.1016/j.celrep.2016.01.023

Meng, X., Zhou, J., Tang, J., Li, B., de Oliveira, M. V. V., Chai, J., He, P., & Shan, L. (2016). Ligand-Induced Receptor-like Kinase Complex Regulates Floral Organ Abscission in Arabidopsis. *Cell reports*, *14*(6), 1330-1338. https://doi.org/10.1016/j.celrep.2016.01.023

Monshausen, G. B., Messerli, M. A., & Gilroy, S. (2008). Imaging of the Yellow Cameleon 3.6 indicator reveals that elevations in cytosolic Ca2+ follow oscillating increases in growth in root hairs of Arabidopsis. *Plant Physiol*, *147*(4), 1690-1698. https://doi.org/10.1104/pp.108.123638

752 Niederhuth, C., Patharkar, O. R., & Walker, J. (2013). Transcriptional profiling of the Arabidopsis
753 abscission mutant hae hsl2 by RNA-Seq. *BMC Genomics*, *14*(1), 37.
754 http://www.biomedcentral.com/1471-2164/14/37
755 Olsson, V., Joos, L., Zhu, S., Gevaert, K., Butenko, M. A., & De Smet, I. (2018). Look Closely, the Beautiful
756 May Be Small: Precursor-Derived Peptides in Plants. *Annu Rev Plant Biol*.
757 https://doi.org/10.1146/annurev-arplant-042817-040413
758 Patharkar, O. R., Gassmann, W., & Walker, J. C. (2017). Leaf shedding as an anti-bacterial defense in
759 Arabidopsis cauline leaves. *PLoS Genet*, *13*(12), e1007132.
760 https://doi.org/10.1371/journal.pgen.1007132
761 Patharkar, O. R., & Walker, J. C. (2015). Floral organ abscission is regulated by a positive feedback loop.
762 *Proc Natl Acad Sci U S A*, *112*(9), 2906-2911. https://doi.org/10.1073/pnas.1423595112
763 Patharkar, O. R., & Walker, J. C. (2016). Core Mechanisms Regulating Developmentally Timed and
764 Environmentally Triggered Abscission. *Plant Physiol*, *172*(1), 510-520.
765 https://doi.org/10.1104/pp.16.01004
766 Poncini, L., Wyrsch, I., Dénervaud Tendon, V., Vorley, T., Boller, T., Geldner, N., Métraux, J. P., &
767 Lehmann, S. (2017). In roots of Arabidopsis thaliana, the damage-associated molecular pattern
768 AtPep1 is a stronger elicitor of immune signalling than flg22 or the chitin heptamer. *PLoS One*,
769 *12*(10), e0185808. https://doi.org/10.1371/journal.pone.0185808
770 Qi, Z., Verma, R., Gehring, C., Yamaguchi, Y., Zhao, Y., Ryan, C. A., & Berkowitz, G. A. (2010). Ca2+
771 signaling by plant Arabidopsis thaliana Pep peptides depends on AtPepR1, a receptor with
772 guanylyl cyclase activity, and cGMP-activated Ca2+ channels. *Proc Natl Acad Sci U S A*, *107*(49),
773 21193-21198. https://doi.org/10.1073/pnas.1000191107
774 Ranf, S., Eschen-Lippold, L., Pecher, P., Lee, J., & Scheel, D. (2011). Interplay between calcium signalling
775 and early signalling elements during defence responses to microbe- or damage-associated
776 molecular patterns. *Plant J*, *68*(1), 100-113. https://doi.org/10.1111/j.1365-
777 313X.2011.04671.x
778 Ranf, S., Grimmer, J., Poschl, Y., Pecher, P., Chinchilla, D., Scheel, D., & Lee, J. (2012). Defense-related
779 calcium signaling mutants uncovered via a quantitative high-throughput screen in Arabidopsis
780 thaliana. *Mol Plant*, *5*(1), 115-130. https://doi.org/10.1093/mp/ssr064
781 Robatzek, S., Chinchilla, D., & Boller, T. (2006). Ligand-induced endocytosis of the pattern recognition
782 receptor FLS2 in Arabidopsis. *Genes Dev*, *20*(5), 537-542. https://doi.org/10.1101/gad.366506
783 Roberts, J. A., Whitelaw, C. A., Gonzalez-Carranza, Z. H., & McManus, M. T. (2000). Cell Separation
784 Processes in Plants- Models, Mechanisms and Manipulation. *Annals of Botany*, *86*, 223-235.
785 Rzemieniewski, J., Leicher, H., Lee, H. K., Broyart, C., Nayem, S., Wiese, C., Maroschek, J., Camgöz, Z.,
786 Lalun, V. O., Djordjevic, M. A., Vlot, A. C., Hückelhoven, R., Santiago, J., & Stegmann, M. (2022).
787 Phytocytokine signaling integrates cell surface immunity and nitrogen limitation. *bioRxiv*,
788 2022.2012.2020.521212. https://doi.org/10.1101/2022.12.20.521212
789 Sanders, D., Brownlee, C., & Harper, J. F. (1999). Communicating with calcium. *Plant Cell*, *11*(4), 691-
790 706. https://doi.org/10.1105/tpc.11.4.691
791 Santiago, J., Brandt, B., Wildhagen, M., Hohmann, U., Hothorn, L. A., & Butenko, M. A. (2016).
792 Mechanistic insight into a peptide hormone signaling complex mediating floral organ
793 abscission. *Elife.*, *5*. https://doi.org/10.7554/eLife.15075
794 Scherzer, S., Maierhofer, T., Al-Rasheid, K. A. S., Geiger, D., & Hedrich, R. (2012). Multiple calcium-
795 dependent kinases modulate ABA-activated guard cell anion channels. *Mol Plant*, *5*(6), 1409-
796 1412. https://doi.org/10.1093/mp/sss084
797 Schindelin, J., Arganda-Carreras, I., Frise, E., Kaynig, V., Longair, M., Pietzsch, T., Preibisch, S., Rueden,
798 C., Saalfeld, S., Schmid, B., Tinevez, J.-Y., White, D. J., Hartenstein, V., Eliceiri, K., Tomancak, P.,
799 & Cardona, A. (2012). Fiji: an open-source platform for biological-image analysis. *Nat Methods*,
800 *9*(7), 676-682. https://doi.org/10.1038/nmeth.2019
801 Shi, C.-L., von Wangenheim, D., Herrmann, U., Wildhagen, M., Kulik, I., Kopf, A., Ishida, T., Olsson, V.,
802 Anker, M. K., Albert, M., Butenko, M. A., Felix, G., Sawa, S., Claassen, M., Friml, J., & Aalen, R.

803 B. (2018). The dynamics of root cap sloughing in Arabidopsis is regulated by peptide signalling.
804 *Nat Plants*, *4*(8), 596-604. https://doi.org/10.1038/s41477-018-0212-z
805 Smakowska-Luzan, E., Mott, G. A., Parys, K., Stegmann, M., Howton, T. C., Layeghifard, M., Neuhold,
806 J., Lehner, A., Kong, J., Grunwald, K., Weinberger, N., Satbhai, S. B., Mayer, D., Busch, W.,
807 Madalinski, M., Stolt-Bergner, P., Provart, N. J., Mukhtar, M. S., Zipfel, C., . . . Belkhadir, Y.
808 (2018). An extracellular network of Arabidopsis leucine-rich repeat receptor kinases. *Nature*,
809 *553*(7688), 342-346. https://doi.org/10.1038/nature25184
810 Somssich, M., Bleckmann, A., & Simon, R. (2016). Shared and distinct functions of the pseudokinase
811 CORYNE (CRN) in shoot and root stem cell maintenance of Arabidopsis. *J Exp Bot*, *67*(16), 4901-
812 4915. https://doi.org/10.1093/jxb/erw207
813 Steinhorst, L., & Kudla, J. (2013). Calcium and reactive oxygen species rule the waves of signaling. *Plant*
814 *Physiol*, *163*(2), 471-485. https://doi.org/10.1104/pp.113.222950
815 Stenvik, G. E., Tandstad, N. M., Guo, Y., Shi, C. L., Kristiansen, W., & Holmgren, A. (2008). The EPIP
816 peptide of INFLORESCENCE DEFICIENT IN ABSCISSION is sufficient to induce abscission in
817 Arabidopsis through the receptor-like kinases HAESA and HAESA-LIKE2. *Plant Cell.*, *20*.
818 https://doi.org/10.1105/tpc.108.059139
819 Sto, I. M., Orr, R. J., Fooyontphanich, K., Jin, X., Knutsen, J. M., Fischer, U., Tranbarger, T. J., Nordal, I.,
820 & Aalen, R. B. (2015). Conservation of the abscission signaling peptide IDA during Angiosperm
821 evolution: withstanding genome duplications and gain and loss of the receptors HAE/HSL2.
822 *Front Plant Sci*, *6*, 931. https://doi.org/10.3389/fpls.2015.00931
823 Taylor, I., & Walker, J. C. (2018). Transcriptomic evidence for distinct mechanisms underlying abscission
824 deficiency in the Arabidopsis mutants haesa/haesa-like 2 and nevershed. *BMC Res Notes*,
825 *11*(1), 754. https://doi.org/10.1186/s13104-018-3864-x
826 Torres, M. A., & Dangl, J. L. (2005). Functions of the respiratory burst oxidase in biotic interactions,
827 abiotic stress and development. *Curr Opin Plant Biol*, *8*(4), 397-403.
828 https://doi.org/10.1016/j.pbi.2005.05.014
829 Vie, A. K., Najafi, J., Liu, B., Winge, P., Butenko, M. A., Hornslien, K. S., Kumpf, R., Aalen, R. B., Bones,
830 A. M., & Brembu, T. (2015). The IDA/IDA-LIKE and PIP/PIP-LIKE gene families in Arabidopsis:
831 phylogenetic relationship, expression patterns, and transcriptional effect of the PIPL3 peptide.
832 *Journal of Experimental Botany*, *66*(17), 5351-5365. https://doi.org/10.1093/jxb/erv285
833 Wang, Y., Li, X., Fan, B., Zhu, C., & Chen, Z. (2021). Regulation and Function of Defense-Related Callose
834 Deposition in Plants. *Int J Mol Sci*, *22*(5). https://doi.org/10.3390/ijms22052393

835

836

Main figures - A dual function of the IDA peptide in regulating cell separation and modulating plant immunity at the molecular level

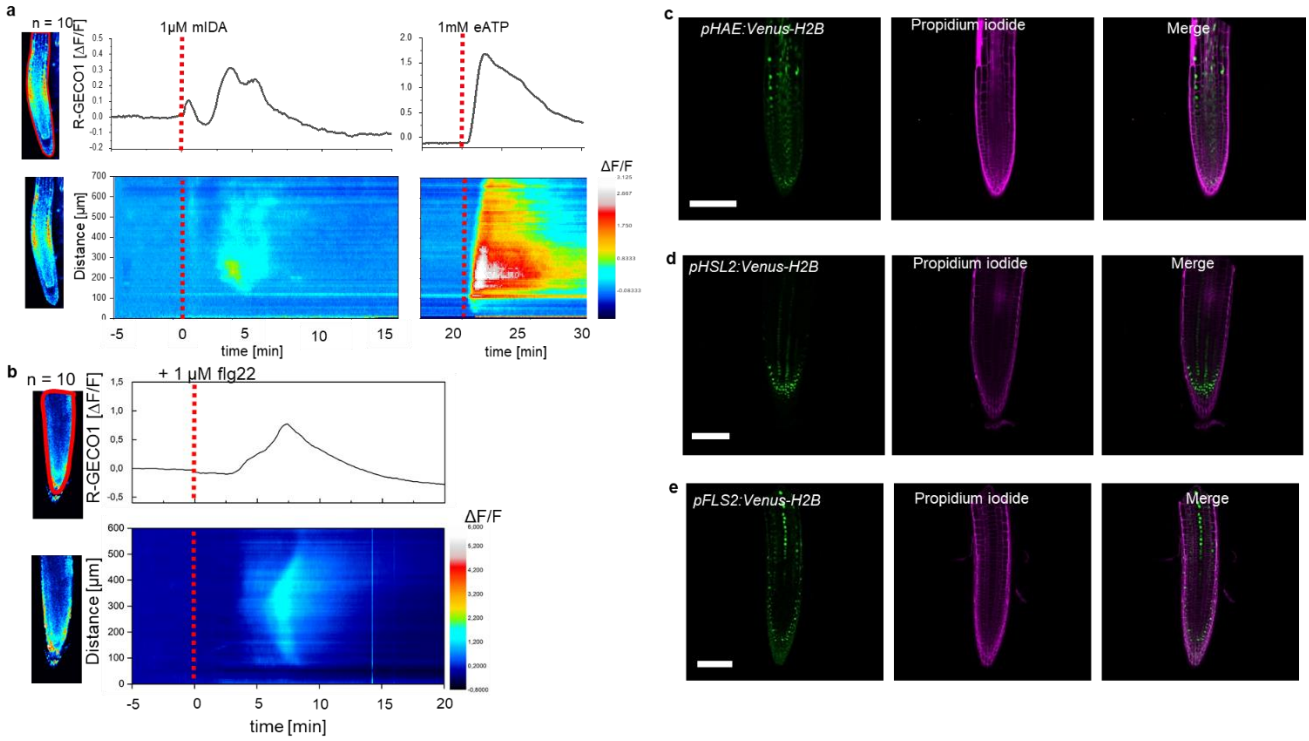

Fig. 1: mIDA-induced $[Ca^{2+}]_{cyt}$ release in Arabidopsis roots correlates with *pHAE* and *pHSL2* activity

a, Normalized R-GECO1 fluorescence intensities (ΔF/F) were measured from regions of interest (ROI) (upper panel, outlined in red) in the meristematic and elongation zone of the root. Fluorescence intensities (ΔF/F) over time of the whole root represented in a heat map (lower panel). Shown are cytosolic calcium concentration ($[Ca^{2+}]_{cyt}$) dynamics in the ROI in response to 1 mM mIDA over time. (see also Movie 1). Red lines at 5 minutes (min) indicates application of mIDA peptide or application of eATP at 22 min. Representative response from 10 roots. The increase in $[Ca^{2+}]_{cyt}$ response propagates through the roots as two waves. **b,** For comparison; Normalized R-GECO1 fluorescence intensities (ΔF/F) measured from regions of interest (ROI) (outlined in red, upper panel) in response to 1µM flg22 over time. Fluorescence intensities (ΔF/F) over time of the whole root represented in a heat map (lower panel). Red line at 0 min (min) indicates application of flg22 peptide. Representative response from 10 roots. The increase in $[Ca^{2+}]_{cyt}$ response propagates through the roots as a single wave seen as normalized R-GECO1 fluorescence intensities (ΔF/F) shown as a heat map (see also movie 2). **c,d,e,** Expression of the receptors **c**, *pHAE:Venus-H2B* **d**, *pHSL2:Venus-H2B* and **e**, *pFLS2:Venus-H2B* in 7 days-

855 old roots. Representative pictures of n = 8. Scale bar = 50 µm, single plane image, magenta = propidium
856 iodide stain.

857

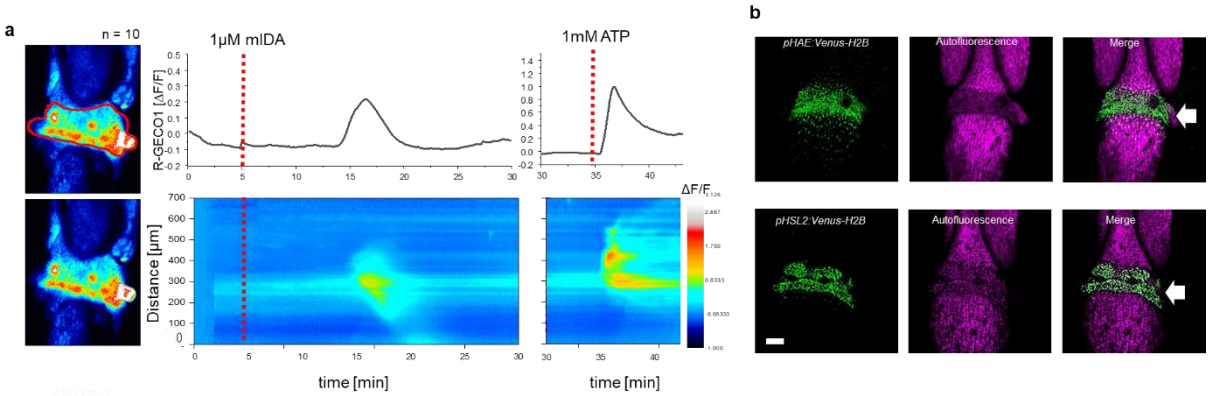

858

859 **Fig. 2 : mIDA-induced $[Ca^{2+}]_{cyt}$ release in Arabidopsis abscission zones.**

860 **a**, Normalized R-GECO1 fluorescence intensities (ΔF/F) were measured from regions of interest (ROI)
861 (outlined in red) in floral abscission zone (AZ)s. Shown are cytosolic calcium concentration ($[Ca^{2+}]_{cyt}$)
862 dynamics in the ROI in response to 1 µM mIDA over time (see also Movie 3). Representative response
863 from 10 flowers. Red lines at 5 minutes (min) indicates application of mIDA peptide or application of
864 eATP at 35 min (for AZs), respectively. The increase in $[Ca^{2+}]_{cyt}$ response propagates through the AZ as a
865 single wave. **b**,Expression of *pHAE:Venus-H2B* and *pHSL2:Venus-H2B* in flowers at position 6 (See Sup
866 Fig. 4a for positions) (arrowhead indicates AZ). Representative pictures of n = 8, scale bar = 100 µm,
867 maximum intensity projections of z-stacks. **b** Expression of *pHAE:Venus-H2B* and *pHSL2:Venus-H2B* in
868 flower position 6 (See Sup. Fig.4a for positions) (arrowhead indicates AZ). Representative picture of n =
869 8. Scale bar = 100 µm, maximum intensity projections of z-stacks.

870

871

872

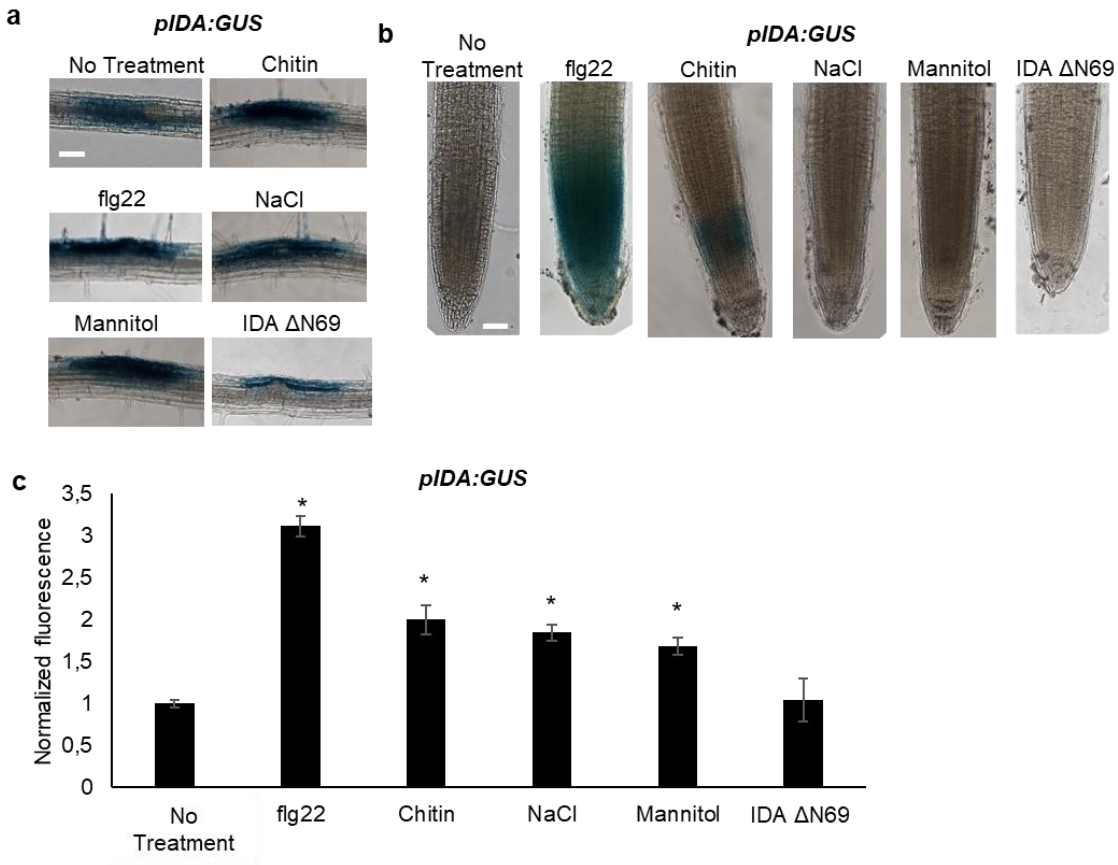

873

874 Fig. 3: *IDA* is induced by biotic and abiotic stress

875 Representative pictures of *pIDA:GUS* expression after 12 h treatment with 1 µM flg22, chitin, NaCl,
876 Mannitol and 1 µM IDAΔN69 in **a,** cells surrounding emerging lateral roots, and **b,** in the main root . **c**,
877 Normalized emitted fluorescence of fluorochrome 4-methyl umbelliferone (4-MU) in 7 days-old
878 seedlings after 12 h treatment with 1 µM flg22, chitin, NaCl, Mannitol and 1 µM of the inactive IDA
879 peptide, IDAΔN69. Normalized to 1 on No Treatment sample. Controls were not subjected to any stimuli
880 (No treatment). n = 6, experiment repeated 3 times. * = significantly different from the non-treated (No
881 treatment) sample ($p < 0.05$, student t-test, two tailed). Controls were not subjected to any stimuli (No
882 treatment). **a,b**, Representative picture of n = 10, experiment repeated 3 times, scale bar = 50 µm.

883

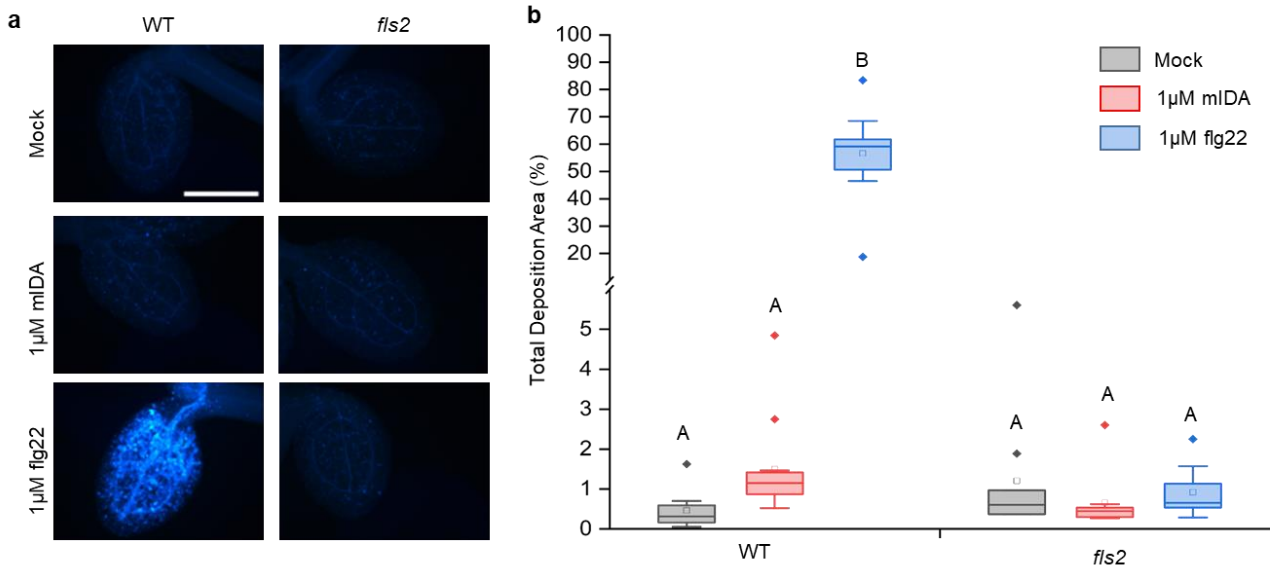

Fig. 4: Callose deposition is not induced by mIDA

a, No callose deposition could be detected in Col-0 WT and *fls2* mutants treated with water (mock treatment) or 1 µM mIDA. Callose deposition could be observed in cotyledons of eight day old Col-0 WT seedlings treated with 1 µM flg22. No callose deposition could be detected in *fls2* mutant treated with flg22. Representative images of 9-12 seedlings per genotype. **b**, Total callose deposition area for the different genotypes treated with water (mock treatment), 1 µM mIDA or 1 µM flg22. Statistical significant difference at ($p < 1*10^{-6}$). N = 9-12

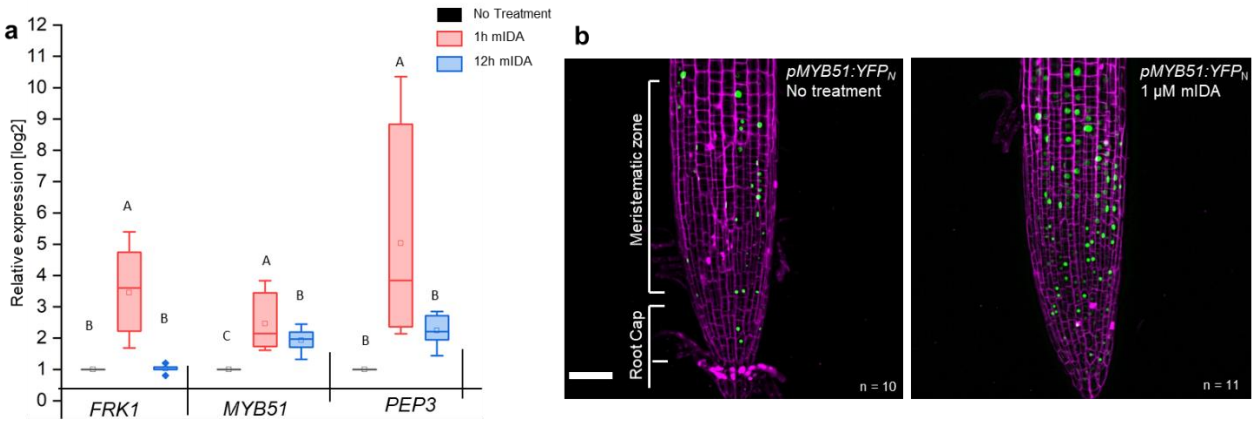

Fig. 5: mIDA induced expression of defense-associated marker genes

a, Transcripts of *FRK1*, *MYB51*, and *PEP3* in WT Col-0 seedlings exposed to 1 µM mIDA for 1 h (light gray) and to 1 µM mIDA for 12 h (dark gray) compared to untreated tissue (black). RNA levels were measured by RT-qPCR analysis. *ACTIN* was used to normalize mRNA levels. n = 4, three biological replicates Statistical analyses was performed comparing induction times of individual genes using one-way ANOVA and post-hoc Tukey's test ($p < 0.05$). **b**,*pMYB51:YFPN* expression is enhanced in roots after 7 h exposure to 1 µM mIDA peptide compared to untreated roots (control), scale bar = 50 µm, maximum intensity projections of z-stacks, magenta = propidium iodide stain.

904

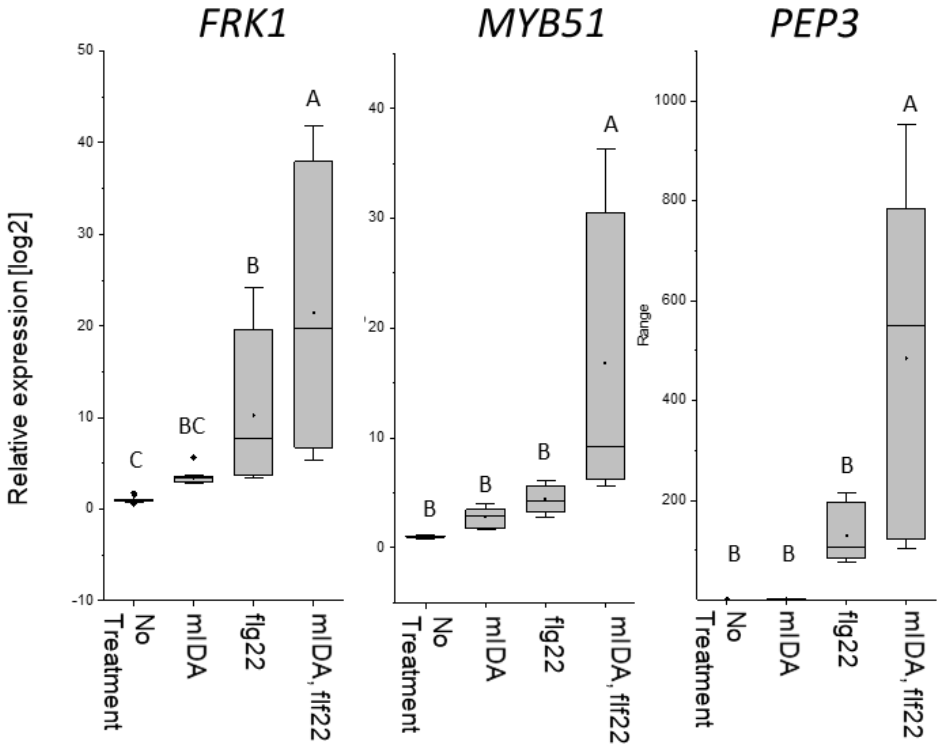

905

906 Fig. 6: mIDA and flg22 co-treatement extremely enhances the expression of defense-associated marker
907 genes

908 a, RT-qPCR data showing transcription of *FRK1*, *MYB51*, and *PEP3* in Col-0 WT seedlings exposed to 1
909 µM mIDA, 1 µM flg22 or a combination of 1 µM mIDA and 1 µM flg22 for 1 h compared to untreated
910 seedlings (No treatment control). *ACTIN* was used to normalize mRNA levels. Figure represent 3
911 biological replicates with 4 technical replicates. Statistical analyses comparing No Treatment to peptide
912 treated samples was performed using one-way ANOVA and post-hoc Tukey's test ($p < 0.05$).

913

914

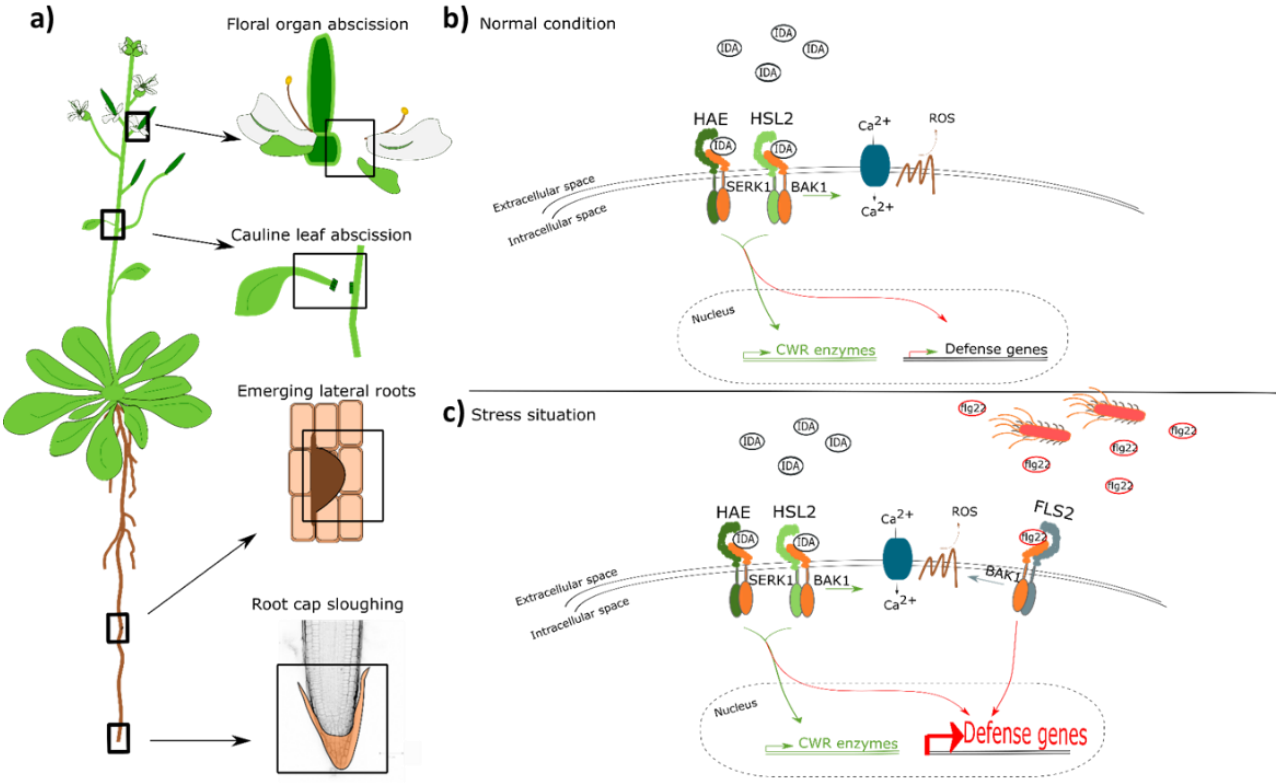

915

916 **Fig. 7: IDA regulates cell separation processes, but is also involved in major transcription of defense**
917 **genes upon pathogen attack.**

918 **a,** IDA and the IDL peptides control cell separation processes during plant development and in response
919 to abiotic and biotic stress (Butenko et al. 2003; Patharkar and Walker 2016; Patharkar et al. 2017; Shi
920 et al. 2018). Tissue undergoing cell separation includes floral organ abscission, cauline leaf abscission,
921 emerging of lateral roots and root cap sloughing. **b**, During normal conditions, IDA control floral organ
922 abscission and emergence of lateral roots by relaying a signal through receptor complexes including
923 HAE, HSL2, SERK1 and BAK1 to modulate the expression of cell wall remodeling (CWR) genes as well as
924 moderately expression of defense genes. IDA activates a receptor dependent production of ROS and an
925 increase in $[Ca^{2+}]_{cyt}$. **b,** Upon stress, such as pathogen attack, the activation of HAE and HSL2 acts in
926 addition to activation of defense related receptors, such as FLS2, to enhance the expression of defense
927 related genes significantly. This ensure optimal protection of cells undergoing cell separation, which
928 may be major entry routes during a pathogen attack.

929

930

Supplementary figures - A dual function of the IDA peptide in regulating cell separation and modulating plant immunity at the molecular level

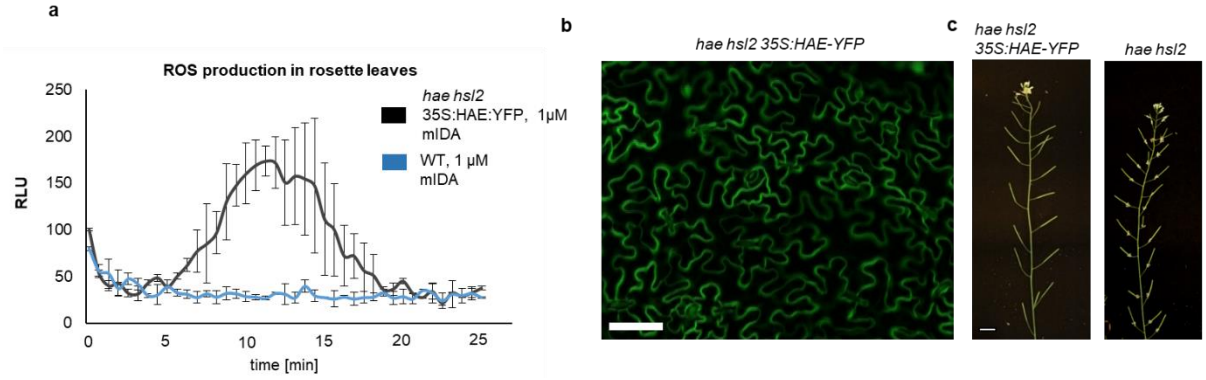

Sup Fig. 1: IDA induces a production of ROS in Arabidopsis

a, ROS production detected by the luminol-based assay was monitored over time as RLU. ROS production from *hae hsl2* leaf disks expressing *35S:HAE-YFP* in response to 1 µM mIDA (black) and in WT control (blue). **b**, Fluorescent image of *hae hsl2* rosette leaves expressing *35S:HAE:YFP*. Signal is detected in the plasma membrane of cells in the epidermal layer. Representative picture. Scale bar = 50 µm. **c**, *35S:HAE-YFP* complements the *hae hsl2* mutant abscission phenotype of observed. Scale = 1 cm.

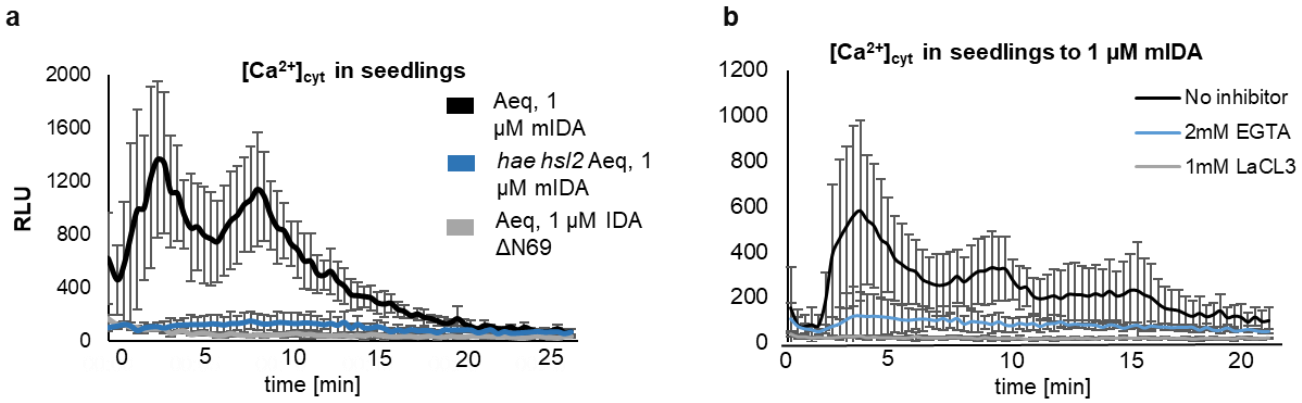

946

947 **Sup Fig. 2 : The IDA triggered increase in** $[Ca2+]_{cyt}$ **is receptor dependent and is abolished in the**

948 **presence of** Ca^{2+} **inhibitors**

949 **a,** Increase in $[Ca^{2+}]_{cyt}$ in seedlings expressing the cytosolic localized *Aequorin*-based luminescence Ca^{2+}

950 sensor (*Aeq*) measured in relative light units (RLU) treated with 1 µM mIDA (black). No response is

951 observed in *Aeq* seedlings treated with 1 µM IDAΔN69 (gray) or in *hae hsl2 Aeq* seedlings treated with

952 1 µM mIDA (blue). **b,** Increase in $[Ca^{2+}]_{cyt}$ in seedlings expressing the cytosolic localized *Aequorin*-based

953 luminescence Ca^{2+} sensor (*Aeq*) measured in relative light units (RLU) treated with 1 µM mIDA . No

954 response is observed in *Aeq* seedlings treated with 1 mM EGTA (blue) or 1mM $LaCl_3$ (grey). Curves

955 represent average of 3 independent experiments with 4-6 replicates in each experiment.

956

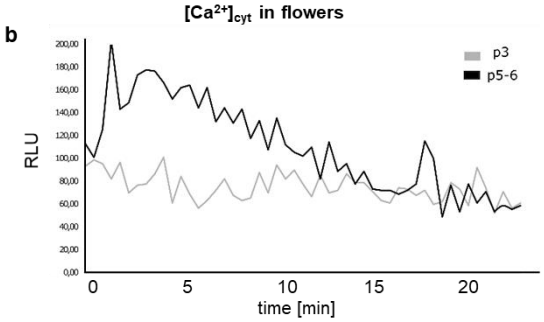

Sup Fig. 3: mIDA induces a Ca^{2+} response in flowers

a, Arabidopsis flowers and siliques at different developmental stages. Flowers along the main inflorescence are counted from the first flower with visible white petals at the top of the inflorescence and is defined as p 1. Subsequently older flowers along the inflorescence (p0-p8). Cell wall remodeling in AZ cells, accompanied with a reduction in petal breakstrength (the force required to remove a petal from the receptacle) is initiated at p6 (red arrow). By p7 AZ cells have undergone cell separation and the floral organs have abscised. p=position **b**, Increase in $[Ca^{2+}]_{cyt}$ in flowers expressing the cytosolic localized *Aequorin*-based luminescence Ca^{2+} sensor (*Aeq*) measured in relative light units (RLU) treated with 1 µM mIDA. A $[Ca^{2+}]_{cyt}$ increase is observed in flowers where there is an initial weakening of the cell walls (p5-6) (black). No increase in luminescence was observed in *Aeq* expressing flowers of an earlier developmental stage (p3) (gray). Curves show representative measurements. Three independent experiments were performed with 4-6 replicates in each experiment.

971

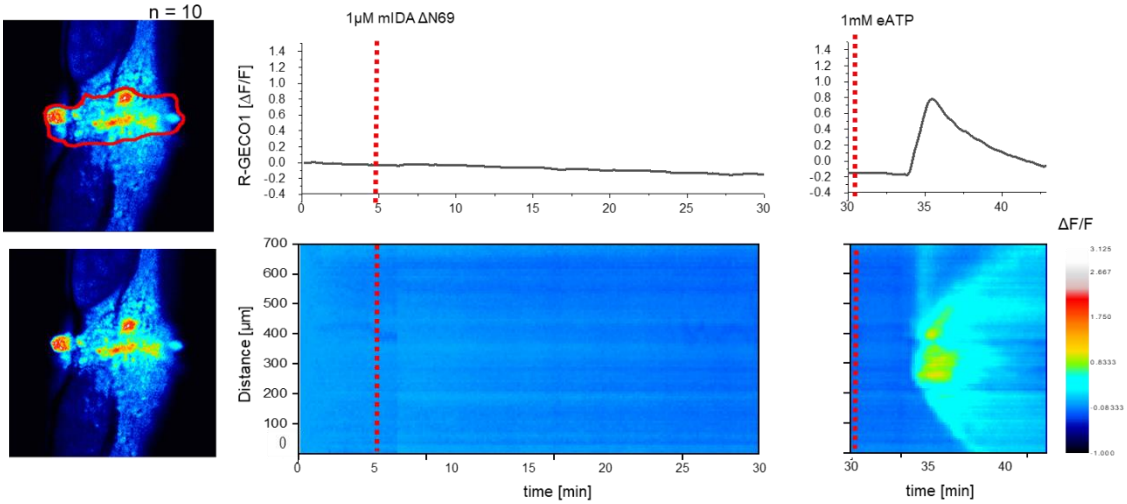

972

973 **Sup Fig. 4: mIDAΔN69 does not induce a $[Ca^{2+}]_{cyt}$ release in Arabidopsis abscission zones (AZ)**

974 Normalized R-GECO1 fluorescence intensities (ΔF/F) were measured from regions of interest (ROI)
975 (outlined in red) in the floral AZs. Shown are cytosolic calcium concentration ($[Ca^{2+}]_{cyt}$) dynamics in the
976 ROI in response to application of 1 µM mIDAΔN69 or eATP over time. Red lines at 5 minutes (min)
977 indicates application of mIDAΔN69 peptide or application of eATP at 30 min (see also Movie 4).
978 Representative response from 10 flowers. The increase in $[Ca^{2+}]_{cyt}$ response to eATP propagates
979 through the AZ as a single wave seen as normalized R-GECO1 fluorescence intensities (ΔF/F) shown as
980 a heat map.

981

982

983

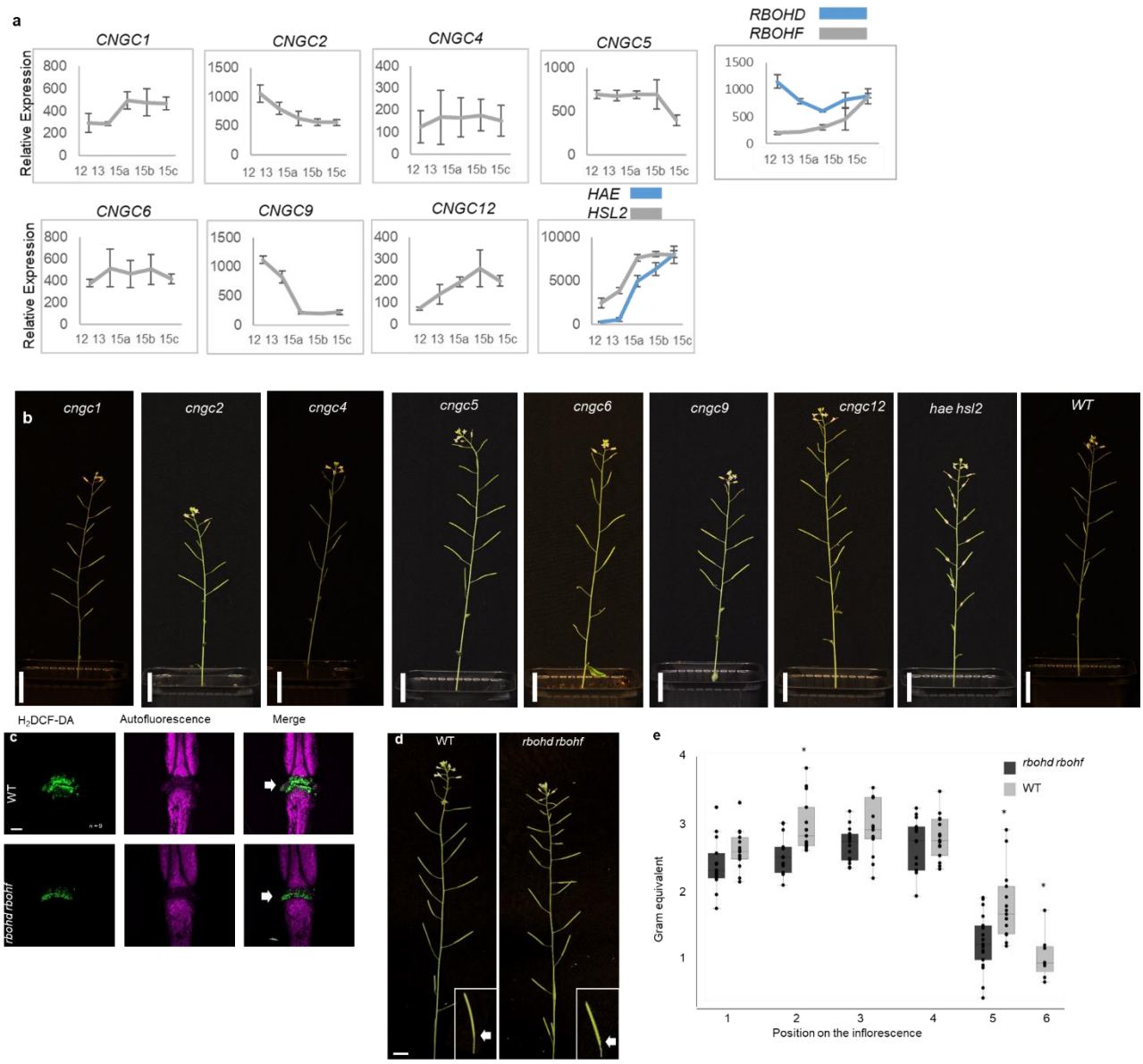

984

985

986 Sup Fig. 5: Investigation of CNGCs and RBOHs in the abscission process

987 **a,** Relative expression of *CNGC1*, *CNGC2*, *CNGC4*, *CNGC5*, *CNGC6*, *CNGC9*, *CNGC12, RBOHD* and *RBOHF*
988 in the floral organs during the onset of abscission (Cai and lashbrook 2008). X-axis represents the
989 developmental stages of abscission where position 12 represent flowers where the stamen and petals
990 are of the same length, position 13 represent flowers at anthesis, position 15 represent flowers with
991 stigma extended above the anthers. Floral organ abscission occurs at position 15. Relative expression
992 of *HAE* and *HSL2* added for comparison. Nomenclature for the abscission process and relative
993 expression values taken from (Cai and Lashbrook 2008). **b**, No floral organ abscission phenotype is
994 observed in the single *cngc* mutant plants compared to the *hae hsl2* mutant which retains the floral
995 organ indefinitely. Scale bar = 2cm, 5 weeks old plants. **c**, ROS production in the AZ (white arrow head)

996 detected by using the fluorescent dye H_2DCF-DA in WT and *rbohd rbohf* flowers at position 6 (See
997 Supplementary Fig. 5a for positions). Scale bar = 100 µm, maximum intensity projections of z-stacks.
998 Representative pictures from 9 flowers. **d**, Representative pictures of WT and *rbohd rbohf*
999 inflorescences, scale bar for inflorescences = 1 cm. **e**, Petal break strength (pBS) measurements of WT
1000 and the *rbohd rbohf* mutant at position 1-6 along the inflorescence. Force required to remove petals
1001 from the receptacle represented in gram equivalent. * = significantly different from WT at the given
1002 position ($p < 0.05$, student t-test, two tailed).

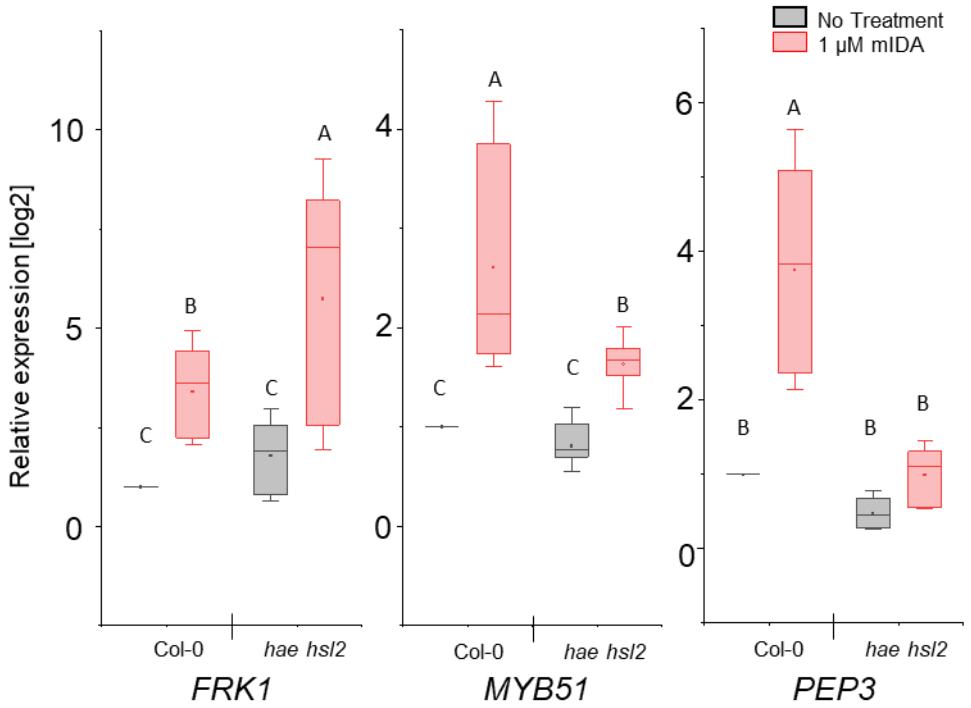

1003

1004 **Sup Fig 6: mIDA induced expression of defense-associated marker genes is only partially dependent on**
1005 **the HAE and HSL2 receptors**

1006 RT-qPCR data showing transcription of *FRK1*, *MYB51*, and *PEP3* in Col-0 WT and *hae hsl2* seedlings
1007 exposed to 1 µM mIDA for 1 h compared to untreated seedlings (No treatment). *ACTIN* was used to
1008 normalize mRNA levels. Figure represent 3 biological replicates with 4 technical replicates. Statistical
1009 analyses was performed comparing samples within same gene, using two-way ANOVA and post-hoc
1010 Tukey's test ($p < 0.05$).

1011

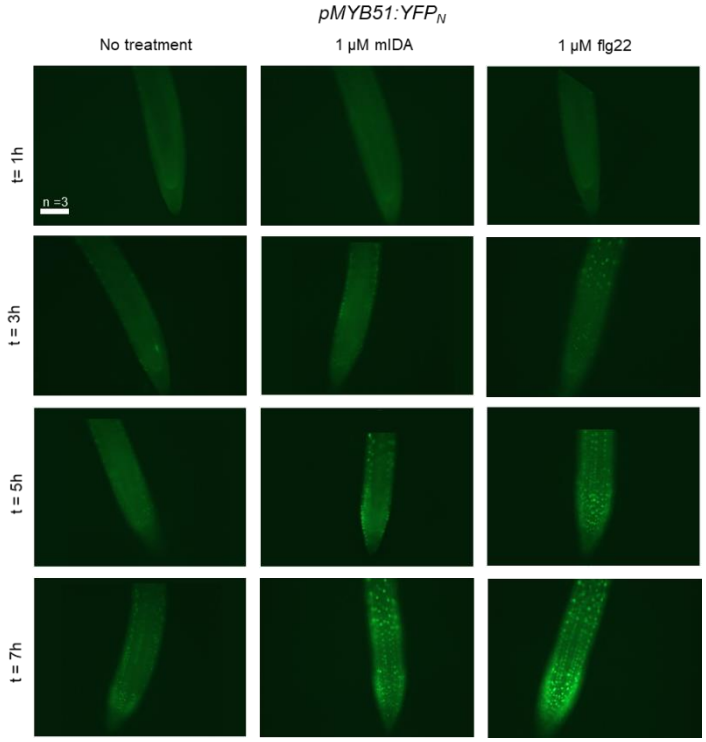

1012

1013

1014 Sup Fig. 7: mIDA and flg22 induced expression of *pMYB51:YFP*

1015 Representative microscopic pictures of 7-days-old *pMYB51:YFPN* roots from seedlings transferred to
1016 liquid medium with 1 µM flg22 or 1 µM mIDA for 1, 3, 5 and 7 h using a fluorescent microscope.
1017 Control seedlings were transferred to medium with no peptide and imaged in the same time frame.
1018 Fluorescent nuclei could be observed in a similar temporal pattern in roots subjected to mIDA and
1019 flg22. Scale bar = 100 µm, single plane images using a Zeiss Axioplan2 microscope with an AxioCam
1020 HRc, 20x air objective and a YFP filter (Excitation: 500/20, Beamsplitter: FT515, Emission: 535/50), no
1021 imaging processing was performed, t = time in h. n = 3, experiment repeated 3 times.

1022

1023

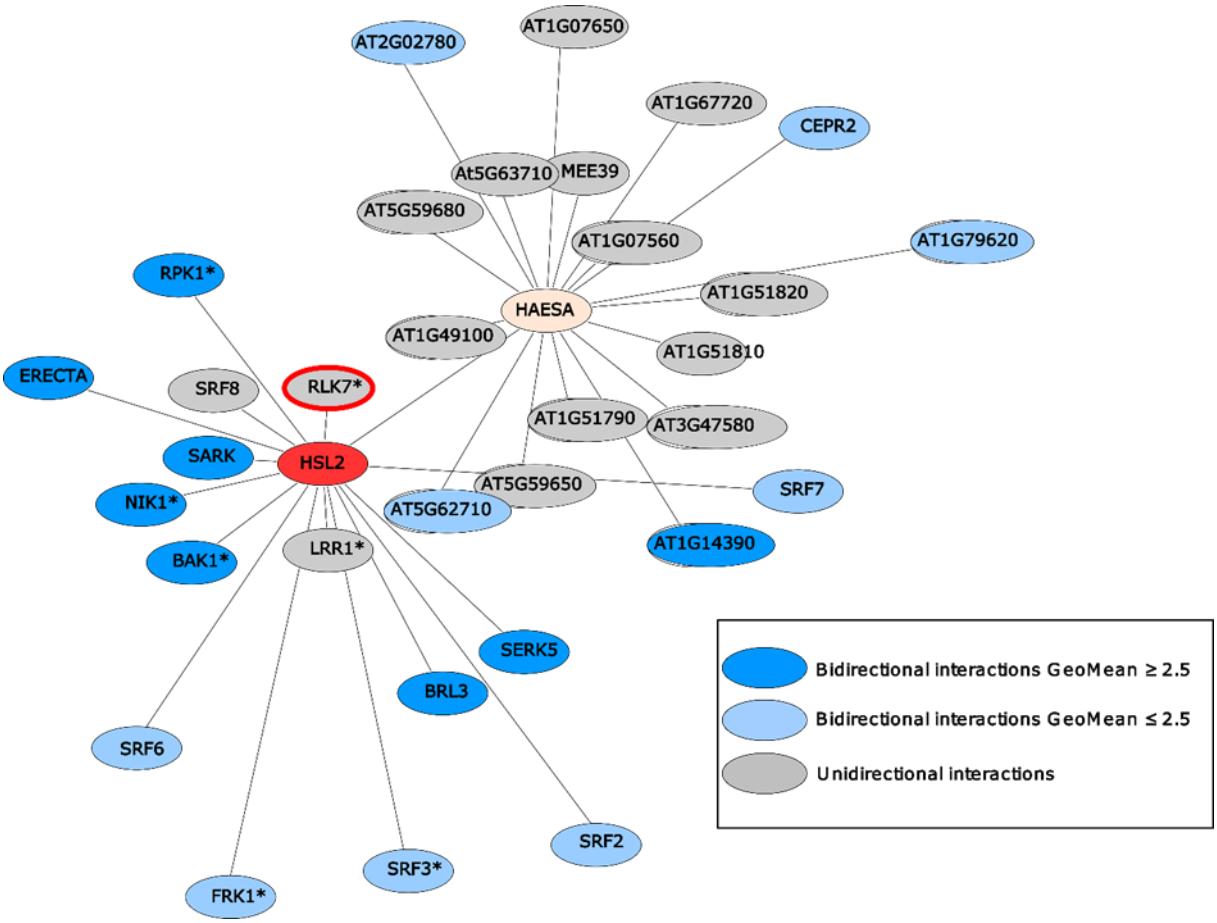

Sup Fig. 8: HAE (yellow) and HSL2 (red) display very distinct repertoire of immune and growth-related interacting LRR-RKs.

HEA and HSL2 specific interacting partners determined using a sensitized high-throughput extracellular domain interaction assay (Smakowska-Luzan et al,.2018). HSL2 and HAE show distinct interacting LRR-RKs where only HSL2 was found to interact with RLK7 (red halo). * indicates receptors known to play a function in biotic and/or abiotic responses in planta based on previous published work, dark blue nodes refer to bidirectional interactions with GeoMean ≥2.5, light blue nodes- refer to bidirectional interactions with GeoMean ≤2.5, and grey nodes refer to unidirectional interactions.